Characterization of the Flow Field Response to Vaneless Space Reduction in Centrifugal Compressors

by

Alfonso D. VillanuevaV.

B.S. Instituto Tecnológico y de Estudios Superiores de Monterrey, México (2000)

Submitted to the Department of Aeronautics and Astronautics in partial fulfillment of the degree of

Master of Science

at the

MASSACHUSETTS INSTITUTE OF TECHNOLOGY

May 26, 2006

Author _____

Department of Aeronautics and Astronautics

May 26,2006

Certified by _____

Choon S. Tan

Senior Research Engineer, Gas Turbine Laboratory

Thesis Supervisor

Certified by _____

Jaime Peraire

Professor of Aeronautics and Astronautics

Chair, Committee on Graduate Students

AERO

Characterization of the Flow Field Response to Vaneless Space Reduction in Centrifugal Compressors

By

Alfonso D. Villanueva

Submitted to the Department of Aeronautics and Astronautics on May 26, 2006 in partial fulfillment of the requirements for the Degree of Master of Science

ABSTRACT

The unsteady three-dimensional flow field for two centrifugal compressors of nearly identical design (one with a marginally smaller impeller-diffuser gap) is interrogated to assess the difference in the time averaged performance and unsteady loading characteristics of the impeller blades. Computational calculations are conducted for three different operating points. Results show that the difference in the time-average performance of the two compressors is due to the change in the level of loss and blockage generated from a difference in the strength of the impeller-diffuser interaction between the two compressors. The unsteady component of loading on the impeller blade originates from pressure waves propagating with a phase difference on the suction and pressure surfaces of the blades. The frequency of the waves is set by the diffuser vanes passing frequency and the wavelength by the product of the diffuser vane passing period and the speed of the wave. It is demonstrated that the difference in static pressure from the pressure surface to the suction surface at the leading edge of the diffuser vanes sets the amplitude of unsteady loading on the blades of the impeller. The level of pressure on both surfaces of the diffuser vane at the leading edge is determined by the value of the local angle of incidence. It is concluded that for a given diffuser design, changes in the impeller configuration or impeller-diffuser gap that result in a variation of the diffuser incidence will lead to a different unsteady loading distribution on the blades of the impeller.

Thesis Supervisor: Choon S. Tan

Title: Senior Research Engineer, Gas Turbine Laboratory

ACKNOWLEDGEMENTS

The realization of this work would not have been possible without the sponsorship of the Mexican National Council for Science and Technology (CONACYT).

Partial support to fund the operations at the GTL for this project came from the GUIDE III Consortium under subcontract 127235-1150027 to the Air Force Prime contract F33615-01-C-2186 with Dr. C Cross as the Contract Monitor and with Dr. J. Griffins as subcontract monitor via Carnegie-Mellon University.

I am grateful to my advisor, Dr. Choon Tan for providing guidance and orientation through the difficult world of research. The contributions of Dr. J. Liu from Honeywell ES&S were crucial in the understanding of MSU TURBO and in the realization of this work. I am also grateful to Dr. J. Adamczyk who helped me build a better understanding of CFD and to Caitlin Smythe for all the answers to my endless questions.

A very special thanks goes to my office mate Mr. Francois Le Floch who not only helped me overcoming many theoretical challenges but who also made the long days at the GTL seem shorter. I would also like to mention Mr. Jerome Bert for all the fun times at the GTL and in general to my Lab friends: Sean, Barbara and Marisa.

A special recognition is dedicated to my brother, Luis Villanueva for encouraging me in completing a Master's program at MIT. My sister Lia, for bringing unforgettable times through long distance phone conversations and to Alison Cathles, who made me not to forget that life is nothing but a bunch of magical instants.

Finally, a special dedication goes to the people who once dreamed of a better world and who have not stopped fighting to see me in it: my parents. Thanks Mom, thanks Dad.

Table of Contents

Nomenclature

Abbreviations

a	Speed of sound
A_{eff}	Effective area of a uniform flow representation of a non-uniform flow.
e_t	Specific stagnation energy
ETE	Euler Turbine Equation
HCF	High cycle fatigue
IDI	Impeller-Diffuser Interaction
LE	Leading edge
PS	Pressure surface
P_r	Rotor pitch: 2π / number of blades in rotor
P_s	Rotor pitch: 2π / number of blades in stator
R	Gas constant
RPM	Revolutions per minute
SS	Suction surface
T_{diff}	Period of time it takes one diffuser vane to occupy the same position of the previous vane as seen from the impeller.
T_{imp}	Period of time it takes one impeller blade to occupy the same position of the previous blade as seen from the rotor.
TE	Trailing edge
U_{tip}	Tangential velocity of the impeller measured at its outer radius
V	Absolute velocity
W	Relative velocity

Symbols

α	Incidence angle
χ	Backsweeping angle
δ^*	Displacement thickness
η	Adiabatic Efficiency
λ	Wavelength
Π	Static pressure ratio
Π_t	Stagnation pressure ratio
τ_a	Actual stagnation temperature ratio
Ω	Angular velocity
θ	Flow or vane angle (see subscript)

Subscripts

1	Impeller inlet
2	Impeller outlet
r	Radial direction
t,θ	Tangential direction

List of Figures

List of Tables

CHAPTER 1

Introduction

1.1 BACKGROUND AND MOTIVATION

1.1.1 The Centrifugal Compressor

The centrifugal compressor has a fairly broad range of applications due to its efficient operation and capability in achieving large stage pressure ratios (~4 to 8).

A typical centrifugal compressor (Figure 1.1) consists of two major components: a rotating impeller and a stationary diffuser. Most of the pressure rise is obtained by a change on the fluid potential energy due to a centrifugal force field. Relatively less pressure rise is produced by the deceleration or diffusion of the flow [3].

The main function of the impeller is to impart angular momentum to the flow while changing its motion from axial to radial. The flow leaving the impeller is at a higher pressure and has a swirl compared to the flow at the inlet. The role of the diffuser is then to decelerate the flow and provide a further pressure increase by removing the swirling component of velocity and reducing the radial velocity component. A pressure rise from a diffusing effect is usually harder to attain due to blockage generation (effective flow area reduction) and likelihood of flow separation.

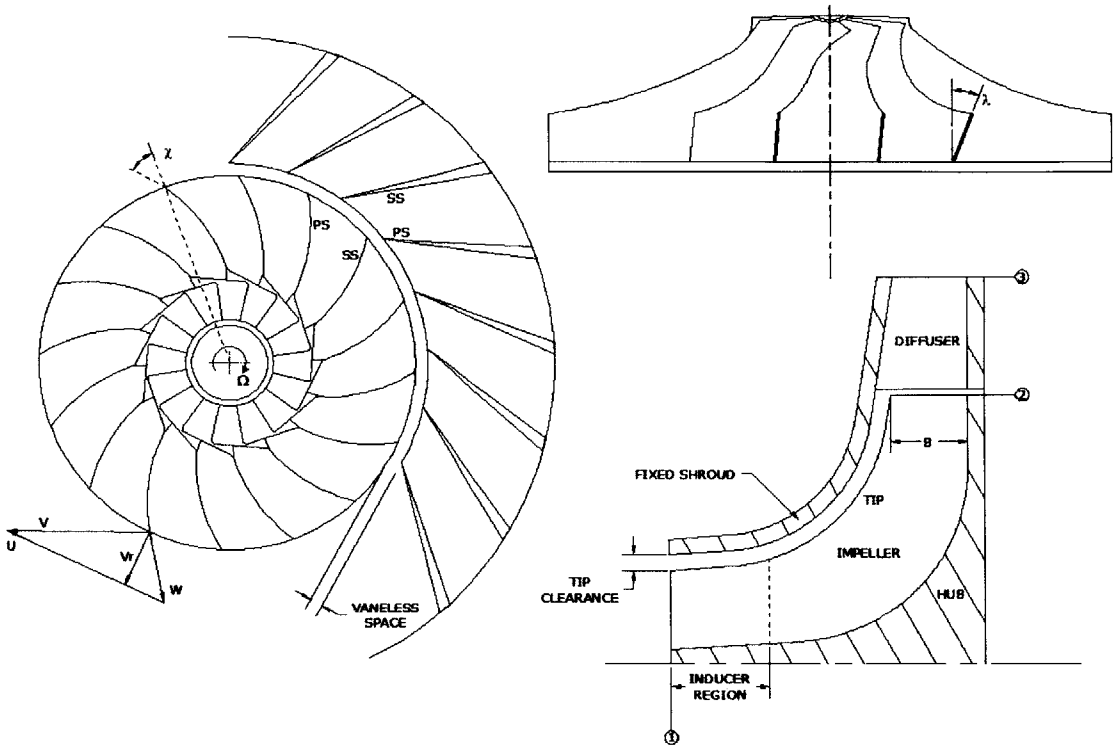

Figure 1.1: Centrifugal Compressor

The flow through the impeller (Figure 1.1) is required to turn from axial to radial as it goes from the inlet to the exit of the impeller. In order to negotiate the turn, the flow is subject to a radial pressure gradient that sets the pressure of the streamlines moving close to the tip of the blades to be low compared to the streamlines moving at the hub (see Figure 1.1). As the streamlines on the tip approach the exit of the impeller they thus encounter an adverse pressure gradient that inevitably results in separation, making the flow to leave the impeller in the form of a jet and a wake [5]. In the inducer region, the blades are shaped in the same manner as those of an axial compressor and provide the flow with a pressure increase. Also, and as shown by Figure 1.1, the blades of the impeller are curved in the radial plane. This feature known as backsweeping, has the purpose of decreasing the effective outflow area and reducing the absolute tangential velocity of the flow. For the same amount of work to be done over the fluid, an impeller with backsweeping would need to rotate faster than an impeller without.

The blades of the impeller may be bound at the tip by a shroud or run close to a fixed casing with a small gap clearance, in which case the impeller is said to be unshrouded. Unshrouded impellers are lighter and introduce less mechanical stresses over the blades. For this reason unshrouded impellers are used for aeronautical applications. Also, shorter blades or splitters are included at the outer portion of the impeller to reduce blade loading. The splitter blades extend from half the meridional distance to the exit of the impeller in order to avoid area obstruction at the inlet, where choking is a possibility.

The diffuser of a centrifugal compressor is usually of the vaned type. This removes some of the friction loss when compared to vaneless diffusers because the flow is decelerated through a shorter path. The optimal operation of a vaned diffuser relies on the correct alignment of the flow with its vanes (incidence angle). The most severe cause of poor performance is probably a result of flow mismatch between impeller and diffuser operation[1]. Vaned diffusers impose unsteady loading on the blades of the impeller due to the unsteady impeller-diffuser interaction effects. As a consequence of the interaction, flows leaking from one impeller passage to the adjacent passage through the clearance at the tip become more pronounced with additional losses due to mixing.

The vaneless space plays a major role. It is known that a reduction in the impeller-diffuser gap results in performance enhancement; however this can lead to severe vibration in impeller blades.

Centrifugal compressors may attain pressure ratios as high as 8:1 in a single stage. Their operation is efficient and stable because they rely on the centrifugal effect for pressurization. It is their rather large frontal area that makes them unattractive when compared to axial compressors where the same pressure ratio is reached through many stages but at a reduced frontal area.

1.1.2 High Cycle Fatigue

Blade vibration is a concern in modern compressor design. It leads to the formation of mechanical cracks and the eventual failure of the blades. This phenomenon is a potential

source of High Cycle Fatigue (HCF) and its effects are of importance for the blades of the rotor.

The known sources of vibration are of two kinds: forced vibration and flutter. Forced vibration exists as the blades of the rotor are subjected to non-uniform flow. These non-uniform regions are in the form of wakes or stationary pressure fields usually imposed by the adjacent blade rows. The frequency at which these vibrations occur is a multiple of the rotor passing frequency and it may lead to situations of resonant response when the value is close to the natural frequency of the blades. When stall cells are present, forced vibration may also take place but at a different frequency from that of the passing vane. Flutter is a self induced aeromechanical instability. The presence of flutter in axial compressors is common but less so in the situation of centrifugal compressors.

If no damping exists, the blades of a rotor oscillate at their natural frequency or harmonics. The specific displacement pattern associated to each of these frequencies is known as the "mode". Since a blade can oscillate in a flexural (F), rotational (R) or Edgewise (E) fashion, there are three main types of modes. When motion is of a mixed type, the resulting mode is however of a more complex structure. This is the case for the blades in a centrifugal compressor, where the definition of flexural or rotational displacements is not appropriate.

Forced vibration on the blades of a centrifugal impeller may come from different sources. The most significant is that imposed by the upstream pressure field of the vanes of the diffuser. The rapid deceleration of flow from the impeller exit to the diffuser inlet results in a region of high pressure gradient at the diffuser inlet as indicated by the contours shown in Figure 1.2. If the absolute velocity of the flow exiting the impeller is supersonic, the abrupt deceleration takes the form of a shock. An impinging shock produces a higher blade loading while introducing a content in harmonics[1].

Since the effects of forced vibration are not easy to predict, the use of a simple Campbell Diagram becomes useful at the design stage. A Campbell Diagram plots lines of the excitation frequency derived from the rotor speed and compares them to the different frequencies of the blade modes to check for crossings (see figure 2.1). While a Campbell

Diagram may be useful in predicting operational points to avoid, it does not include information about the actual levels of vibration. To complete this task, new methodologies are currently under study and make use of a combination of Computational Fluid Dynamics (CFD) with Finite Element analysis (FEA).

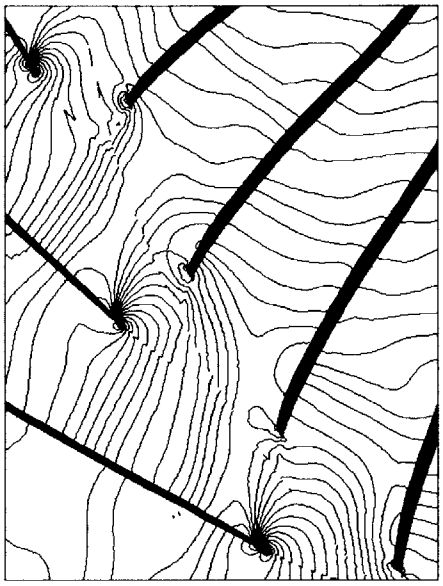

Figure 1.2: Static Pressure contours on the vicinity of Impeller and Diffuser Vanes

1.1.3 CFD-FEA models

Unsteady CFD simulations are employed to obtain the value of static pressure acting on the surfaces of a blade at a particular time. From FEA, the mode shapes and natural frequencies of the blades are computed. It is required to know which components of the static pressure act on the direction of the vibrating motion of the blade. Pressure values from CFD are therefore projected onto the mode shapes obtained with FEA. The result is a Generalized Forcing Function (GFF) indicating the net contribution of pressure load to mode vibration [19]. A Fourier analysis is performed over the GFF to spot the different forcing frequencies and their amplitudes. These amplitudes, known as modal forces, are incorporated into the FEA model to determine the actual strains or stresses associated with a specific mode.

1.2 PREVIOUS WORK

Despite the recent focus on centrifugal compressors, increasing progress in their study has been made through a combination of experimental and computational studies.

Early experimentations concentrated on the characterization of the jet-wake model originally proposed by Dean and Senoo [5]. In this model the flow leaving the impeller consists of a jet with high stagnation pressure and a wake with lower stagnation pressure and lower velocity. Laser measurements performed by Eckardt [6] and Krain [7] gave physical evidence for the support of this model. More recent measurements by Ziegler etal [8] centered on the description of the influence of impeller-diffuser interaction (IDI). Ziegler discovered that a reduction in the vaneless space presented two major consequences: a reduction of the separated region exiting the impeller and a higher incidence into the diffuser vanes, this last effect being of primary concern in loading and enhancement of the efficiency.

Significant progress in numerical algorithms and availability of computational resources have enabled applications of CFD to analyze turbomachinery flow. Initial computations were confined to computing steady flow in single passages of isolated blade row or the use of a mixing plane approximation for multi-blade rows. Chen, Adamczyk and Celestina [9] developed a new procedure for the simulation of unsteady flows employing a single blade channel. Their model relies on the assumption that the flow at the bounding limits of a blade passage is periodic in time. The employment of boundary conditions lagging in time or in "phase" makes the simulation of a single passage suffice for the construction of a full wheel representation. Subsequent experiments by Chen [10] proved that this phase-lag procedure renders almost identical results to those of conventional time-accurate techniques but at a much lower computational effort.

Several works have exploited the application of CFD to the study of different aspects of the flow. Dawes [13] and Shum [18] employed CFD to describe impeller-diffuser interaction. Dawes found that the zones of unsteadiness due to IDI are confined to the impeller trailing edge and the diffuser entry zone. He also noticed that spanwise variations of the flow properties have a higher impact on diffuser operation than unsteady effects. Shum made use

of the same code as Dawes to describe the mechanisms through which IDI influences stage performance. His findings pointed to viscous losses from tip leakage flow as well as blockage and slip to be the responsible mechanisms. A reduction of these quantities was found to have a positive influence on the stage performance. Higher IDI (reduced vaneless space) would decrease blockage and slip but would increase the losses. He concluded that the prediction of an optimal vaneless space could be reached by the proper assessment of these factors at the design stage.

Other papers outline the use of CFD in combination with FEA (Finite Element Analysis) to the study of mechanical vibrations on rotor blades. Rabe and Kenyon [15] modeled the loading response of fan blades to distortions in total temperature in the inlet flow finding that a difference in the incidence angle produced a different shock structure that resulted in higher unsteady loading. Mansour and Kruse [14] actually developed a full CFD-FEA model to predict the vibrational strains of a centrifugal compressor. Their model relied on a periodic simplification of the actual geometry and did not quite reproduce test-rig data. Smythe [17] employed phase-lag boundary conditions to study the unsteadiness of loading over the blades of the same compressor. Her findings led to the hypothesis that the difference in the incidence angle of the flow at the inlet of the diffuser affected the pressure pattern of the vaneless space and hence the loading of the impeller blades.

1.3 TECHNICAL OBJECTIVES

The goal of this research is to explain the mechanism in the flow field that can potentially lead to an aeromechanic difficulty on the blades of the impeller of a centrifugal compressor. The specific technical objectives are:

(i) Determine the contribution of unsteady impeller-diffuser interaction to time-averaged performance and identify the causes responsible for this observed time-averaged effect.

(ii) Establish a causal link between the unsteady flow processes due to impeller-diffuser interaction and the unsteady loading characteristics of loading on the impeller blades.

1.4 CONTRIBUTIONS

The contributions of this thesis are two:

1. The characterization of the changes in the flow field of two centrifugal compressors of nearly identical design: one being the production design and the other the enhanced version in which the vaneless space has been reduced by growing the impeller tip radius. The characterization can be described in terms of the two aspects delineated below:

- The difference in the time-average performance (pressure ratio and efficiency) between the two compressors and the quantification of the flow effects responsible for the observed difference, namely the difference in the level of loss and blockage generated from a difference in the strength of the impeller-diffuser interaction between the two designs.

- The unsteady component of loading on the impeller blade originates from pressure waves propagating with a phase difference on the suction and pressure surfaces of the blades. The frequency of the waves is set by the diffuser vanes passing frequency and the wavelength by the product of the diffuser vane passing period and the speed of the wave. It is demonstrated that the difference in static pressure from the pressure surface to the suction surface at the leading edge of the diffuser vanes sets the amplitude of unsteady loading on the blades of the impeller.

2. The level of pressure on both surfaces of the vane is set by the value of the local angle of incidence. The angle of incidence was shown to vary with the point of operation and with compressor design. The difference of incidence angle from the enhanced version to the production version is the result of the changes in the effective impeller channel flow area produced by a different level of impeller-diffuser interaction.

The findings stated above prove the hypothesis originally put forward by Smythe [17].

1.5 THESIS OUTLINE

This thesis is organized as follows:

Chapter 2:

The basic methodology employed to characterize the flow field response to a reduction in the vaneless space is defined in this chapter. First the two compressors that feature as the articles for this research are presented. Then the general features of the CFD code employed in the computation of the flowfield are listed. A brief explanation of the phase lag boundary condition technique and its use in the production of post-processing results is offered. Finally the different methods employed for the averaging of the flow quantities are presented.

Chapter 3:

This chapter describes the analysis followed in the assessment of the time-averaged performance of the two compressors. The actual pressure ratios of the two compressors obtained from CFD calculations are compared to those predicted by ideal approximations. The difference in pressure ratios is explained by the assessment of non-ideal flow mechanisms such as losses and blockage. The stage efficiency of the two compressors is computed and the main differences delineated.

Chapter 4:

The unsteady loading of the impeller blades is characterized in this chapter. Time averaged and unsteady loading distributions are computed for both compressors. Differences in the spatial distribution and loading magnitude are quantified. A detailed investigation on the formation of unsteady loading is performed and the source of unsteadiness is linked to the behavior of the flow field in the diffuser.

Chapter 5:

Summary and conclusions from this research work are presented.

CHAPTER 2

Technical Approach

2.1 ARTICLES OF RESEARCH

The subjects of study for this research are two centrifugal compressors designed and built by Honeywell Engines, Systems and Services. The first compressor forms part of a current production line. The second compressor is an enhanced version which attempted to have a 2% increase in flow capacity and in pressure ratio. Both compressors are referred hereafter as the Production and Enhanced. The Enhanced compressor is not under production. These are the same articles of research that Smythe [17] employed in her study.

The impeller in both compressors consists of 17 main blades and 17 splitter blades. Both compressors are matched to the same diffuser, which is composed of 25 vanes. The impeller tip radius of the Enhanced is 0.5% larger than that of the Production, so that the Enhanced design has a reduced impeller-diffuser gap. This modification results in high stress/strain observed levels in the blades of the impeller of the Enhanced design causing HCF concerns.

On the test rig, the Enhanced compressor showed large vibrational strains when crossing with the 5^{th} splitter blade mode at 96% speed (see Figure 2.1)[21]. The Production compressor also presents crossings, with the 4^{th} splitter mode at 95% speed. The strains at the crossing for the Enhanced compressor were twice as high as that for the Production compressor when measured in the splitter blade (at a location near the hub, see strain seeding in Figure 2.2) . Crossings at lower modes of the Enhanced compressor resulted however in less strain when compared to the Production. This evidence shows a potential difference in the Structural Dynamics of the blades from one compressor to another [14].

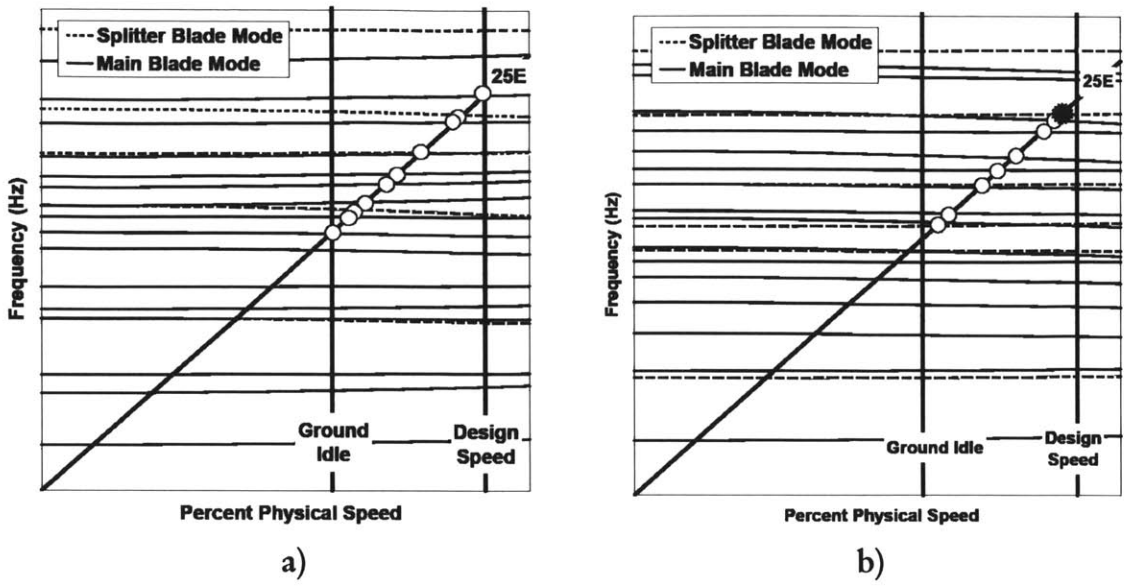

Figure 2.1: Campbell Diagrams for a) Production and b) Enhanced Compressors [21]

Measurements were done by embedding the strain gauges on the surfaces of the blades. Figure 2.2 shows the location of the gauges. Unfortunately, the information on the Enhanced compressor is somewhat inaccurate since the data points are available for only one blade and fail to take into consideration blade to blade variations.

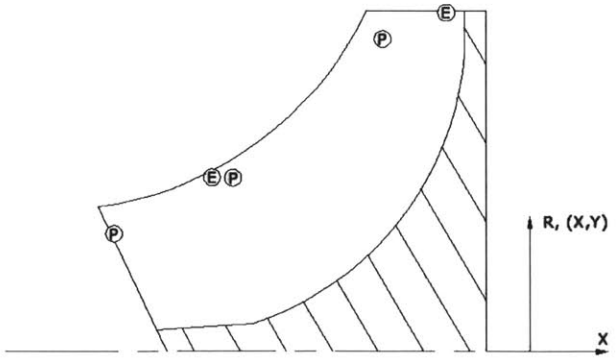

Figure 2.2: Strain gages location for the Production and Enhanced impeller

2.2 NUMERICAL APPROACH

MSU TURBO is the CFD code employed for the computational investigation of the flow field. This multiblock solver was developed at the Mississippi State University by J.P. Chen. It uses a time-accurate implicit method with Jacobi and Gauss-Siedel relaxation to solve three dimensional unsteady Reynolds-Averaged Navier- Stokes Equations (RANS). Discretization is made under a characteristics-based finite-volume scheme. Turbulence model is based on NASA/CMOTT $\kappa-\varepsilon$ model [12].

The governing equations are formulated in the rotating frame of motion. The vectorized equation is:

$$(L+D+U)\Delta q^{k-1} = \frac{q^{n} - q^{k-1}}{\Delta t} + R^{k-1} \tag{2.1}$$

where q is the vector containing the state variables [ρ, ρu, ρv, ρw, e_t]. Two levels of Newton iterations at each instant in time are employed, the inner level is used to solve for the change Δq between iterations and the outer level to solve the linear system expressed by the above Equation. L,D and U are the lower, upper and diagonal matrices derived from the discretization scheme and R is the term grouping body forces and balance of fluxes.

For the present articles of study, MSU TURBO offers two advantages: its parallel processing allows for the possibility of modeling complex centrifugal passages by simple blocks. It also minimizes the computational domain to a single blade passage since it makes use of phase-lag boundary conditions.

Output from TURBO is presented in two standard types: PLOT3D and APNASA. For the current analysis the former is utilized. PLOT3D is a standard adopted after the development of PLOT3D visualization package by NASA (early 90's). The output quantities are the five

state variables normalized by conveniently chosen free-stream values (Table 2.1) . In PLOT3D free stream values are taken as $a_\infty = 1$, and $\rho_\infty = 1$ and the gas constant R=1.

Quantity	Value
Q1	ρ/ρ_∞
Q2	$(\rho u)/(\rho_\infty a_\infty)$
Q3	$(\rho v)/(\rho_\infty a_\infty)$
Q4	$(\rho w)/(\rho_\infty a_\infty)$
Q5	$(\rho e_t)/(\rho_\infty a^2_\infty)$

Table 2.1: PLOT3D standard normalization scheme

Unsteady calculations are performed by partitioning time in finite instants called time steps. The accuracy of the calculation is set by specifying the number of time steps per impeller blade passing period (time taken for a blade to complete one impeller pitch). A binary file representing the solution of a particular instant is printed for every block at each time step.

The computational grid employed for both compressors; Production and Enhanced, is composed of four blocks modeling a single impeller passage and a fifth block modeling the diffuser. The vaneless space region is represented by block 4 and the first portion of block 5. Figure 2.3 displays a surface within the grid corresponding to mid-span location. Any node within the grid is identified by its coordinates on a streamline-based system; i.e. streamwise (i), spanwise (j) and pitchwise direction (k). Table 2.2 indicates the total amount of nodes by block.

	PRODUCTION			ENHANCED		
	i	j	k	i	j	k
Block 1	35	51	53	37	51	53
Block 2	134	51	27	134	51	27
Block 3	134	51	27	134	51	27
Block 4	20	51	53	20	51	53
Block 5	103	51	41	97	51	41

Table 2.2: Computational grid dimensions

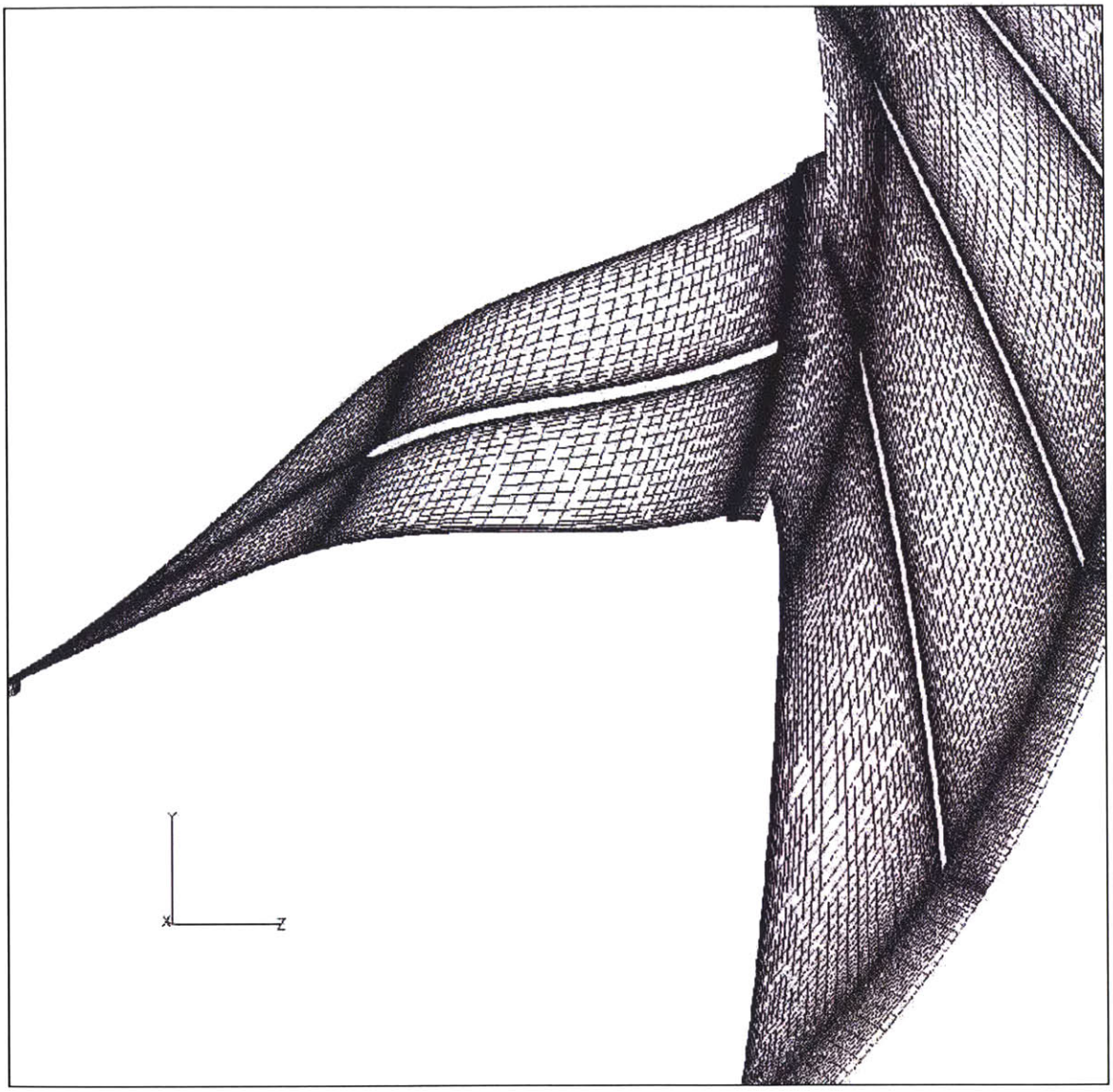

Figure 2.3 Computational grid: surface taken at 50% span-wise. Note that grid consists of only one impeller passage and one diffuser passage, but 3 diffuser channels are shown for graphical purposes.

2.3 PHASE LAG BOUNDARY CONDITIONS AND POST-PROCESSING

In order to make CFD a useful resource, computing times need to be minimized. A classic approach focuses on the simplification of the computational domain (the grid). Spatial periodicity in the solution is frequently used to reduce large domains into simpler ones. If a variable is periodic in space, only the portion in which the variable is periodic is modeled. A full solution can then be constructed for the entire space by repeating the spatially periodic solution. When modeling turbomachinery passages of interacting blade rows, full cascade domains can be reduced to a few blade passages under the assumption that any variable within the flow field will repeat if periodicity in space is present. In such a way a compressor stage of 24 stator blades and 36 rotor blades is modeled by a domain consisting of 2 stator blades and 3 rotor blades (flow field solution repeats 12 times along the full wheel, see Figure 2.4). A fully constrained problem is then defined because the condition in one of the tangential boundaries of the passage is the same as that at the other boundary for all times.

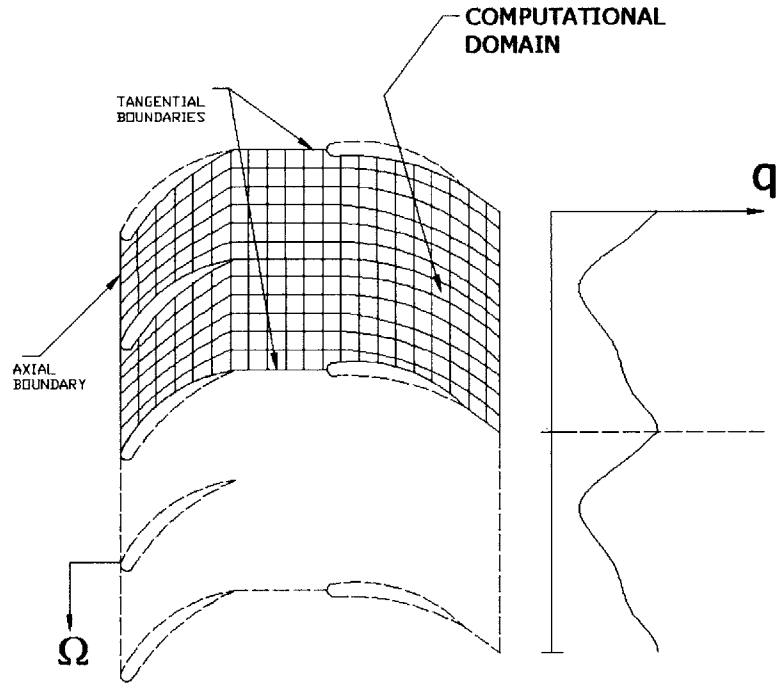

Figure 2.4: Spatially Periodic Flow Field in the modeling of an axial compressor passage. Note: blades do not represent actual orientation.

The Phase lag boundary condition technique relies on a stronger assumption about periodicity: the flow field is also periodic in time. The flow configuration within a turbomachinery passage is only dependent on the relative position of the interacting blade row and it will be the same every time the relative position of the adjacent blade row is repeated (passing period). Although the assumption is not completely accurate, Erdos et al [23] and Chen [10] proved that the unsteady flow field of a passage responds mostly to perturbations caused by the wakes of the interacting blade row. This supposition permits the reduction of the computational domain to a single passage thus saving a large amount of computer memory. There are two beneficial implications of the method:

a) The conditions at the boundaries of the computational domain are known if the flow field evolution within the passage is stored over a time period associated with the adjacent blade row.

b) A full wheel solution can be constructed from the recorded history of the flow within a single passage.

Figure 2.5 illustrates the situation at the boundaries of a stator single passage with an interacting blade row. The condition on boundary 1 at time t1 is that of 2 at a previous time t0. Also the boundary condition on 2 at time t2 is the condition at 1 at time t0. In time t3, when the rotor has rotated one complete passing period, both conditions for 1 and 2 are the same as those at time t0. It is concluded that if the conditions at both boundaries 1 and 2 are known for a complete time period of the adjacent blade row, they will be known at any other instants in time.

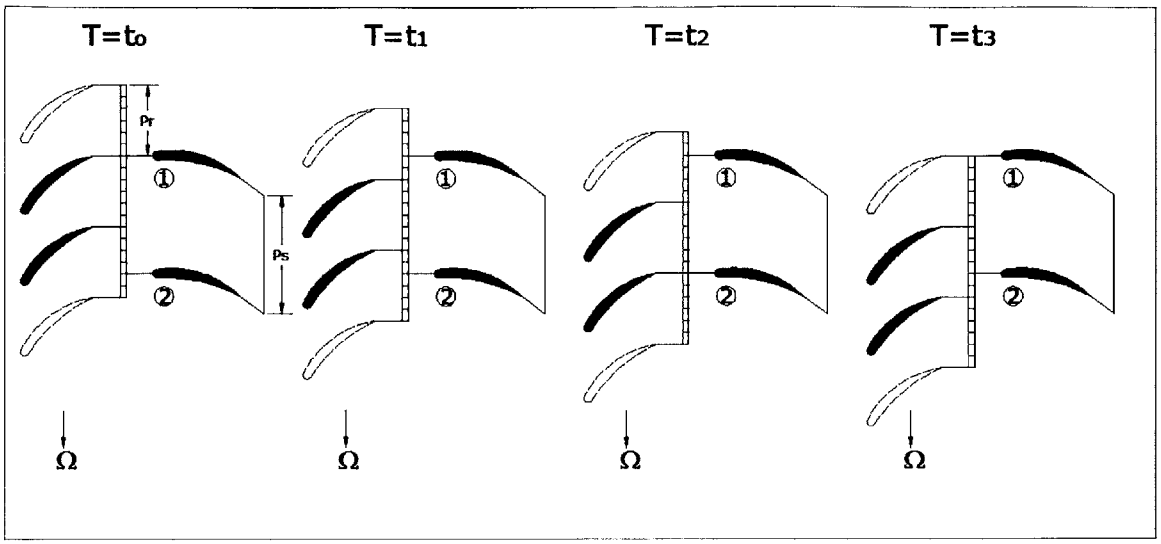

Figure 2.5: Phase lag boundary conditions

In order to know the boundary conditions for the initial period, the flow field is initialized by an average passage approach [24]. The general passage approach states that flow field response to the unsteady interaction of the adjacent row can be decomposed into a sum of a time averaged solution and a term containing the unsteady nature of the response.

$$q(r,\theta,z,t) = \overline{q_{tave}}(r,\theta,z) + \tilde{q}_{pert}(r,\theta,z,t) \tag{2.2}$$

The time-averaged solution can be directly found by solving an average-passage system of equations without involving a time-marching scheme [9]. The perturbations are constructed by taking the adjacent blade row solution and subtracting their axisymmetric averages, then added to the average-passage solution [10]. As a result, the initial condition of the flow field from which subsequent time integration will build up is set. Under the same principle the condition at the axial and tangential boundaries can be computed for every position of the adjacent blade row for a complete time period and then be stored along this interval.

For the current research a post-processor to display full wheel solutions from the results of TURBO was developed using FORTRAN and MATLAB. At a specific instant in time, a full wheel representation is constructed by assigning neighboring passages a solution at other times. The selection of the correct time file to allocate to each passage is better described by Figure 2.6. For a full wheel representation at time t' the actual position of the original passage (m=0) is localized. Neighboring passages are then numbered in the direction of rotation m=1,2,3...N (for both rotor and stator). As stated by the Phase lag boundary conditions technique, the value of any flow variable as seen by the rotor original passage (m=0) at time t=t' is the same at a later instant in time when the rotor has rotated one full stator passage (=Ps/Ω where Ps is the stator pitch $2\pi/N_{statorblades}$, and Ω is the angular velocity of the rotor)

$$q_{r,m=0}(t') = q_{r,m=0}(t' + \frac{\mathrm{P}s}{\Omega} N) \tag{2.3}$$

Where N represents any integer number (N can also be negative meaning a previous instant in time).

The value of a flow variable at an adjacent rotor passage m is the value of a flow variable for the original passage m=0 at a posterior time when the flow passage has moved m rotor pitches.

$$q_{r,m}(t') = q_{r,m=0}(t' + \frac{\mathrm{Pr}}{\Omega} m) = q_{r,m=0}(t' + \frac{\mathrm{P}s}{\Omega} N + \frac{\mathrm{Pr}}{\Omega} m) \tag{2.4}$$

The time at which a solution for the m passage is referred from the original passage is the target time [11] and is simply computed as:

$$t^* = t' + \frac{\mathrm{P}s}{\Omega} N + \frac{\mathrm{Pr}}{\Omega} m \tag{2.5}$$

For the stator, the same principle of repeatability applies but in an opposite direction when transmitting the results of passage m=0 to any other m passage (variations at m=0 happen first in time than for other m's)

$$t^* = t' + \frac{\mathrm{Pr}}{\Omega} N - \frac{\mathrm{Pr}}{\Omega} m \tag{2.6}$$

The post-processor developed for this investigation finds the target time for each one of the passages in the rotor and stator and allocates the corresponding time solution from the original passage.

Additionally to the full-wheel post-processor, many FORTRAN and MATLAB routines were created for the computation of other quantities of interest.

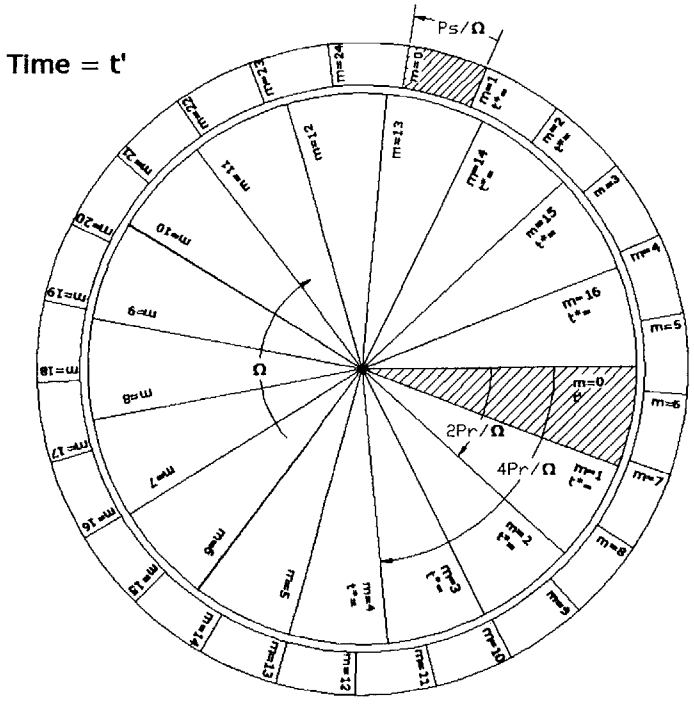

Figure 2.6 : Target Time allocation for full-wheel display

2.4 AVERAGING OF FLOW VARIABLES

In the analysis of the following chapters, averaged flow quantities are employed. The selection of the appropriate averaging technique for the representation of a given flow quantity is presented below:

a) Mass averaging: $\bar{B}^M = \dfrac{\int B\rho u dA}{\int \rho u dA}$

All the velocities in the flow field (u, v, w, v_r, v_θ, W) have been mass averaged throughout the analysis. Mass averaged is employed with the intention of preserving the same amount of mass from the actual flow field to the hypothetical uniform flow. Total Pressure P_t and total Temperature T_t are also mass averaged. The computation of other average quantities such as η, S, or θt is also based on mass averaged values.

b) Area averaging: $\bar{B}^A = \dfrac{\int B dA}{\int dA}$

Static pressure is the only quantity that is area averaged since the representation of an equivalent flow acting on surfaces of the blades must exert the same force as the actual flow.

c) Time Averaging: $\bar{B}^t = \dfrac{\sum_{i=1}^{N} B}{N}$

Any measured quantity at a specific location in space is averaged over time by the formula given above, where N is the total number of time instants over which the quantity is averaged. If the quantity of interest is derived from variables that are time and spatial varying, the mass or area average technique is first applied and then the time-average technique.

2.4 SUMMARY

The current research focuses on the study of two compressors from Honeywell Engines Systems and Services. One of the compressors (the Enhanced) is the redesigned version of the other (the Production). When tested on a rig, the Enhanced compressor presented an unsatisfactory aeromechanic response with large vibrational strains registered at the splitter blade and close to the hub. The analysis here presented is based on the computational simulation of the unsteady flow field of these compressors. The purpose of the analysis is to reveal the nature of the mechanisms produced by impeller-diffuser interaction that set the difference in loading between the two articles of research.

The employed tool is MSU TURBO, a CFD code based on the implementation of phase-lag boundary conditions. A post-processing program in FORTRAN has been developed with the purpose of visualizing full-wheel results.

CHAPTER 3

Time-average Results

3.1 INTRODUCTION

This chapter focuses on comparing the time-average performance of both the Production and the Enhanced compressor. An issue is the impact on the performance change associated with a 0.5% increase in the impeller radius of the Enhanced compressor to that of the Production design. There could be two sources for the observed change: one is associated with the additional work that could be done on the flow due to the increase in the impeller radius and the other is the change in impeller-diffuser interaction due to a reduced impeller-diffuser gap.

The analysis is performed by employing the Euler Turbine Equation (ETE) and the one-dimensional model developed by Shum[18] to account for the change in blockage and loss associated with the time-averaged effect of unsteady impeller-diffuser interaction. Two operation points are chosen to make a comparison between the compressors: MASS1 and MASS2 (see Figure 3.1). Operation at MASS1 corresponds to the operation at the same corrected flow at which the test rig data was collected during the vibration measurements (operation near design). Operation at MASS2 has been strategically chosen near the stall point with the purpose of maximizing the intensity of the unsteady effects [17].

The chapter is organized into four sections. In the first section, the pressure ratios are quantified and Shum's [18] model is introduced. The second and the third section evaluate losses and blockage using Shum's model to determine their effect on pressure change. Finally, stage and impeller efficiency are computed for the two compressors at the two points of operation.

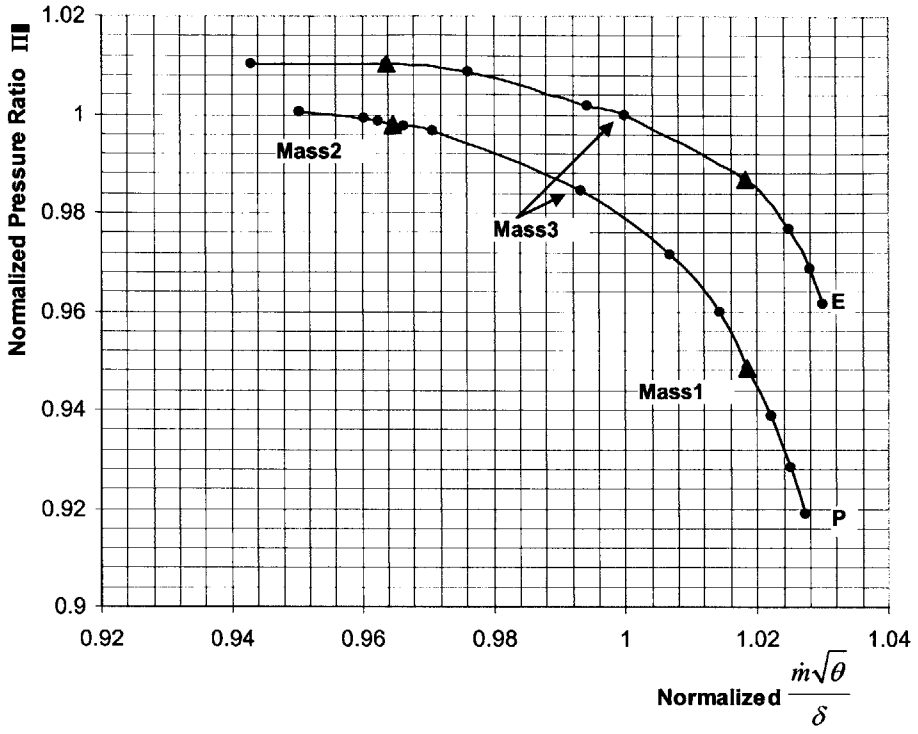

Figure 3.1: Compressor characteristics identifying operation points of interest (Smythe 2005).

3.2 EVALUATION OF PRESSURE RATIOS

3.2.1 Euler Turbine Equation

Euler Turbine Equation (ETE) relates the changes in stagnation temperature of a working fluid to the work done on it by a torque on a compressor. It is derived from the combination of an energy balance and the conservation of angular momentum applied to the compressor. In an adiabatic situation with no losses, the operation of the compressor is assumed to be isentropic and stagnation pressure changes can be related to stagnation temperature changes through an isentropic relation. A derived expression from ETE to compute stagnation pressure changes is then obtained. For a centrifugal compressor with non-swirling flow at

the inlet of the impeller, this relation takes the form of eq. 3.1:

$$\frac{P_{t2}}{P_{t1}} = \left(1 + \frac{V_{t2}U_2}{CpT_{t1}}\right)^{\frac{\gamma}{\gamma-1}} \tag{3.1}$$

From TURBO, total and static properties are averaged (section 2.4) to obtain ratios of total and static pressure. A comparison between the application of ETE and the values obtained from the numerical simulation is presented. All ratios are normalized by the corresponding reference value (total or static) of the Production case at MASS1 obtained by TURBO:

		Mass 1			Mass2		
		Production	Enhanced	Δ %	Production	Enhanced	Δ %
Πt	ETE derived	1.11	1.14	2.8	1.21	1.21	0.03
	CFD	1.00	1.02	2.2	1.02	1.03	1.8
Π	ETE derived	0.98	0.99	1.9	0.98	0.99	1.3
	CFD	1.00	1.03	2.7	1.00	1.02	2.0

Table 3.1: Comparison of total and static pressure ratios obtained from (ETE) and TURBO for both compressors.

The results for both calculations (ETE and TURBO) show higher pressure ratios for the Enhanced compressor. The increment in stagnation pressure ratio at each point of operation predicted by the derived expression from ETE is higher than the actual CFD values from one compressor to another. (This is to be expected as we have assumed ideal adiabatic flow in using ETE to compute total pressure ratio) The trend is the opposite for the values of static pressure which are higher in the CFD calculations. These observations suggest that the change in the level of unsteady interaction between Enhanced and Production may be responsible for the observed change in the time-average performance.

3.2.2 Shum's Model

In his Thesis [18] Shum develops a model to account for changes in pressure ratio (total and static) for centrifugal impellers interacting with upstream vaned diffusers. The starting point is a modified Euler Turbine Equation that accounts for the effect of losses during the compression process:

$$\frac{P_{t2}}{P_{t1}} = \left(1 + \frac{V_{t2}U_2}{CpT_{t1}}\right)^{\frac{\gamma}{\gamma-1}} \cdot e^{\frac{-(\Delta S)}{R}} \tag{3.2}$$

The losses are expressed in terms of entropy changes (see section 3.3 for connecting ΔS to losses). Eq. 3.2 shows only two variables that can be affected by the interaction of an impeller with a vaned diffuser: tangential velocity V_t and ΔS. A linearizing procedure is then applied to the equation so as to isolate the impact of the changes in these variables to the change in Πt. The tangential exit velocity Vt, does not feature as a fully independent variable since it depends on the relative velocity W and the angle of slip [18] (see Fig. 1.1). Furthermore, changes in W are caused by local quantities that by means of a one-dimensional analysis are shown to be the effective flow area A_{eff} and the entropy change ΔS. As an overall result, changes in stagnation pressure ratio between compressors without (vaneless diffusers) and those with interaction (vaned) can be explained by the changes of three quantities: Effective area at the exit of the impeller (A_{eff}), Losses (ΔS) and Slip (-Δθ). Shum's model is expressed in the following equation:

$$\frac{\Delta Pt_2}{Pt_2} = C_a\left(\frac{\Delta A_{eff}}{A_{eff}}\right) + C_s\left(\frac{\Delta S_2}{Cp_0}\right) + C_\theta(-\Delta\theta) \tag{3.3}$$

Where C_a, C_s and C_θ are the coefficients computed from the following formula:

$$C_a = \left(\frac{U_2 - Vt_2}{Vt_2}\right)\left(\frac{1}{1-M_{rel,2}^2}\right)\left(\frac{\gamma}{\gamma-1}\right)\left(\frac{Vt_2U_2}{Cp_oTt_1 + Vt_2U_2}\right)$$

$$C_s = -(1+C_a)\left(\frac{\gamma}{\gamma-1}\right)$$

$$C_\theta = \left(\frac{1}{\tan\alpha}\right)\left(\frac{\gamma}{\gamma-1}\right)\left(\frac{Vt_2U_2}{Cp_oTt_1 + Vt_2U_2}\right)$$

Shum showed that since $C_a > 0$, $C_s < 0$ and $C_\theta > 0$ a higher total to total pressure ratio may be attained if there exists : more effective Area ($A_{eff}\uparrow$), reduced loss ($\Delta S\downarrow$)and reduced slip ($\Delta\theta\downarrow$) [18].

In a similar manner, a one dimensional model for the static pressure incremental change is developed. Since static pressure is not a frame-dependant quantity, Shum develops this model directly using influence coefficients (Shapiro [27]):

$$\frac{\Delta P_2}{P_2} = C_{\tilde{A}}\left(\frac{\Delta A_{eff}}{A_{eff}}\right) + C_{\tilde{S}}\left(\frac{\Delta S_2}{Cp_0}\right) \tag{3.4}$$

With $C_{\tilde{A}}, C_{\tilde{S}}$:

$$C_{\tilde{A}} = \left(\frac{\gamma M_{rel,2}^2}{1-M_{rel,2}^2}\right) > 0$$

$$C_{\tilde{S}} = -(1+C_{\tilde{A}})\left(\frac{\gamma}{\gamma-1}\right) < 0$$

It is concluded that a higher static pressure ratio will also be attained if there is more effective area and lower losses from one compressor to another. The assessment of these quantities will provide further evidence of the Enhanced compressor having pressure ratios larger than that of the Production compressor.

3.3 LOSSES

Losses are associated with entropy production in Turbomachinery passages. For a perfect gas, the change in entropy of a particle going from one state to another may be directly obtained from the combination of Gibbs and the equation of State. The resulting equation is:

$$s_2 - s_1 = Cp \ln\left(\frac{T_{t2}}{T_{t1}}\right) - R \ln\left(\frac{P_{t2}}{P_{t1}}\right) \tag{3.5}$$

If no heat or work is added to the fluid (constant stagnation temperature), a decrease in stagnation pressure is accompanied by an increase in entropy:

$$\frac{P_{t2}}{P_{t1}} = e^{-\frac{\Delta s}{R}} \tag{3.6}$$

Mixing of flows with different characteristics (i.e. velocity, temperature) are examples of situations in a compressor where the action of viscous forces and thermal conduction produce irreversible changes in the flow. Irreversibilities result in entropy production (entropy increase). According to Fig. 3.2 the changes occurring in a compressor can be modeled as the added effect of changes produced reversibly and changes produced irreversibly.

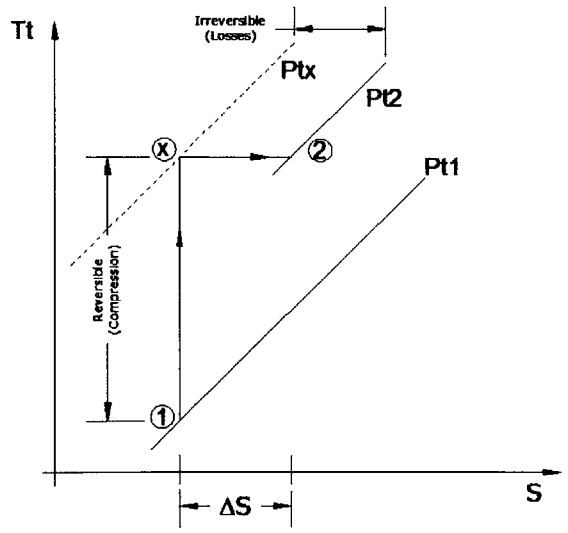

Figure 3.2: Diagram showing the relation of losses to entropy changes

The relation derived from ETE for total-pressure ratio can be modified to account for non-ideal effects:

$$\frac{P_{t2}}{P_{t1}} = \frac{P_{tx}}{P_{t1}} \cdot \frac{P_{t2}}{P_{tx}} = \left(1 + \frac{V_{t2}U_2}{CpT_{t1}}\right)^{\frac{\gamma}{\gamma-1}} \cdot e^{\frac{(S_2 - S_1)}{R}} \tag{3.7}$$

Equation (3.7) constitutes the starting point of Shum's model. As stated by Eq. 3.3 the change of entropy is an important metric in defining the change in pressure ratio of a compressor having stronger impeller-diffuser interaction.

In CFD analysis, it is preferred to compute the rate of change of entropy of a fluid particle along its trajectory. This permits the identification of regions of entropy generation by tracking how the entropy of a fluid particle changes at the different positions along its path. The computation of Ds/Dt for a flow with no heat sources or heat exchange with the surroundings is [2]:

$$\rho \frac{Ds}{Dt} = \frac{1}{T}\tau_{ij}\frac{\partial u_i}{\partial x_j} + \frac{\mathrm{K}}{\mathrm{T}^2}\left(\frac{\partial T_i}{\partial x_j}\right)\left(\frac{\partial T_i}{\partial x_j}\right) \tag{3.8}$$

The results in Table 3.4 make use of eq. 3.5 whereas the plotted contours of Figure 3.3b are based on eq. 3.8.

Boundary layers or regions of high mixing constitute regions of entropy generation. Shum [18] found dense contours of ρDs/Dt in planes close to the trailing edge of the impeller between the tip of the blade and the fixed shroud. To illustrate these contours and their evolution along the impeller channel, successive crossing planes for the Production compressor are displayed in Figure 3.3a at a particular instant in time. The Enhanced compressor shows a similar pattern and for illustration purposes the Production compressor is only displayed. It can be noticed that as the flow approaches the exit, these contours are concentrated in the tip region. In Figure 3.3b, the same contours are displayed for the exit plane of the impeller for the Production and the Enhanced compressor. The results are similar to those found by Shum[18].

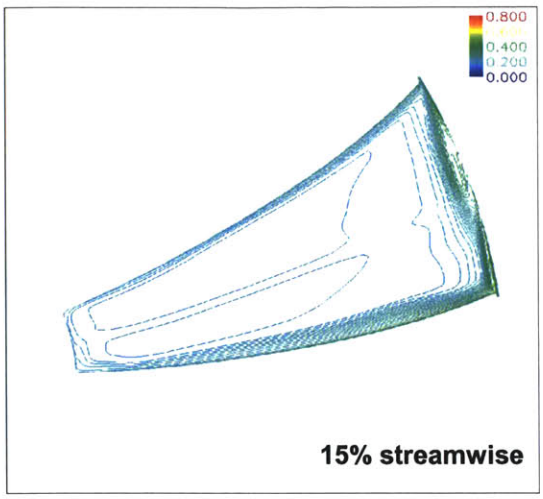

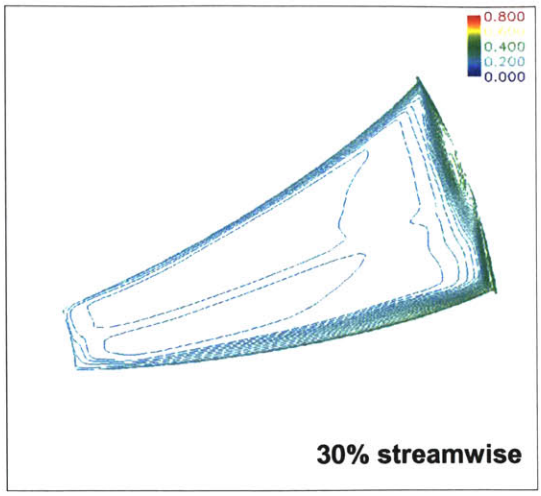

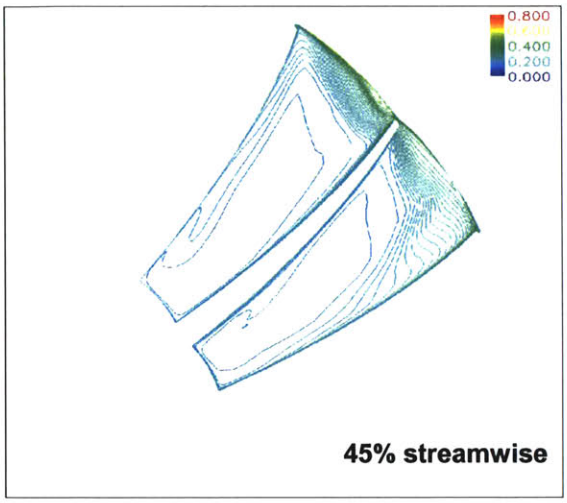

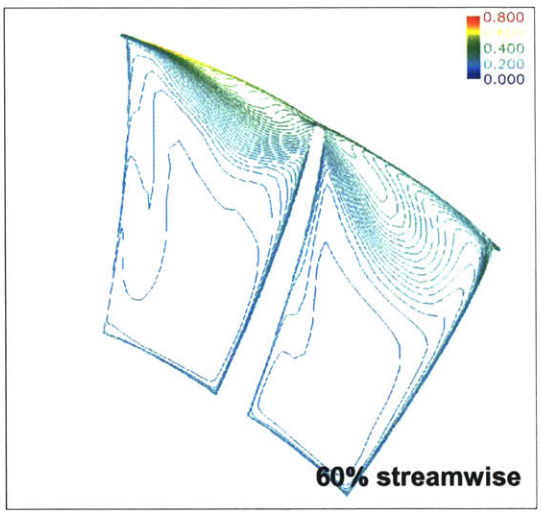

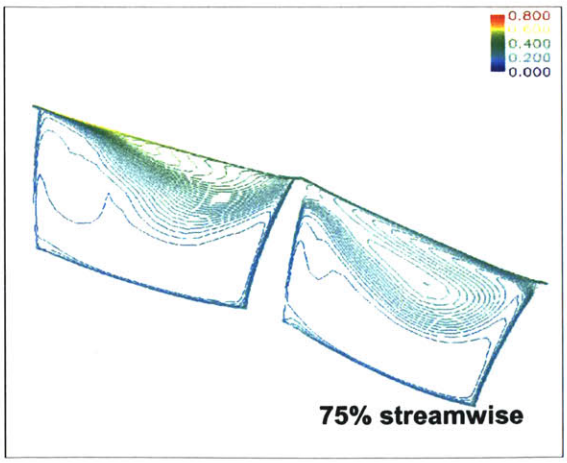

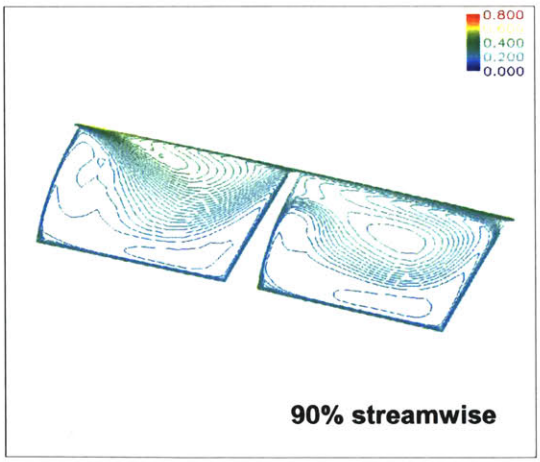

Figure 3.3a Evolution of Entropy contours along impeller passage: Production (values normalized)

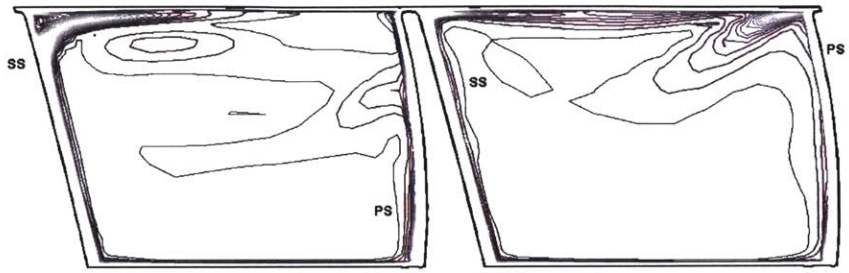

Production

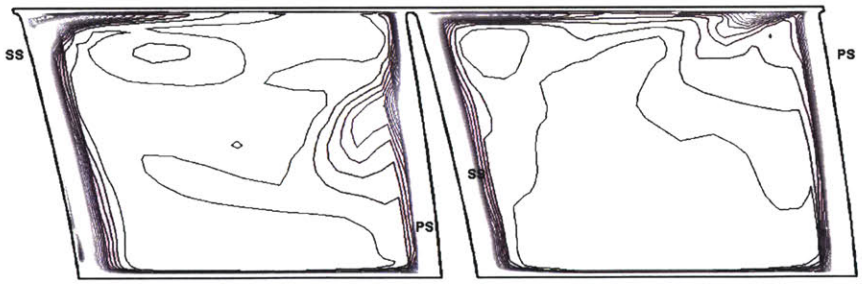

Enhanced

Figure 3.3b: Contours of time-averaged entropy generation ρDs/Dt at the exit plane of the Production and the Enhanced compressor.

The entropy contours were interpreted by Shum as the result of flow leaking from the pressure surface to the suction surface through the clearance at the tip. To prove the existence of tip leakage in the Production and Enhanced compressor, particle paths were traced in regions close to the tip. The trajectories revealed flow migration from the pressure surface to the suction surface (note a line is drawn connecting path vectors):

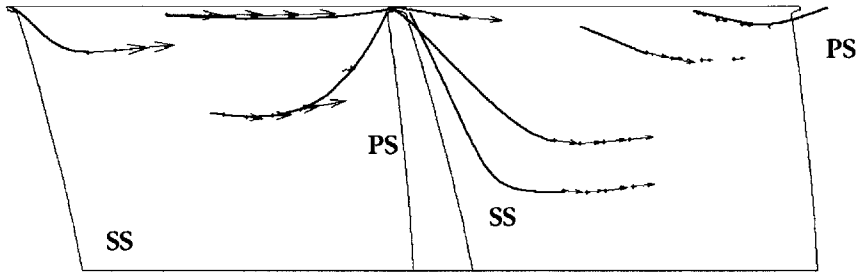

Figure 3.4: Tip leakage flow represented by particle pathlines

By moving onto regions of lower static pressure, the flow coming from the pressure surface will increase its speed with respect to the flow on the suction surface. The entropy production due to tip leakage is explained by the large viscous stresses generated in the shear layer existing between the incoming flow of the pressure surface and the flow at the suction surface (see dissipation term $\tau du/dx$ in eq. 3.8).

The computation of losses obtained for the impeller of both compressors is expressed by entropy changes in Table 3.2:

	Production		Enhanced		
	$\frac{(S_2 - S_1)}{Cp}$	$\frac{T_2(S_2 - S_1)}{0.5V_{t2}U_{tip}}$	$\frac{(S_2 - S_1)}{Cp}$	$\frac{T_2(S_2 - S_1)}{0.5V_{t2}U_{tip}}$	$(S_{enha}-S_{prod} / Cp)=(\Delta S / Cp)$
MASS1	0.0205	0.0884	0.0246	0.1060	0.00408
MASS2	0.0213	0.0921	0.0257	0.1110	0.00439

Table 3.2: Change of entropy for each compressor at each operation point and evaluation of the change from one compressor to another.

For the Enhanced compressor, losses in the impeller are higher when compared to the Production. This effect was originally observed by Shum, and can be explained from the fact that a reduced vaneless gap will lead to a higher impeller-diffuser interaction producing higher tip leakage flow. The viscous dissipation derived from mixing of the tip flow will hence be higher and higher losses will be observed.

3.4 EFFECTIVE AREA AND BLOCKAGE

Flows within turbomachinery passages are subject to the effects of boundary layers and other regions of non-uniform velocity. A typical velocity profile of a viscous flow shows regions of boundary layers close to the walls where velocity is non-uniform and of reduced value compared to the main stream. This type of flow can be modeled as an equivalent non-viscous stream of uniform core velocity passing the same amount of mass through a smaller area (see Figure 3.5). The area of the equivalent stream is thought of as an effective area (A_{eff}) and its difference with the actual area (A) is considered to be a blocked area. The presence of boundary layers and other regions of velocity retardation then constitute regions of flow blockage.

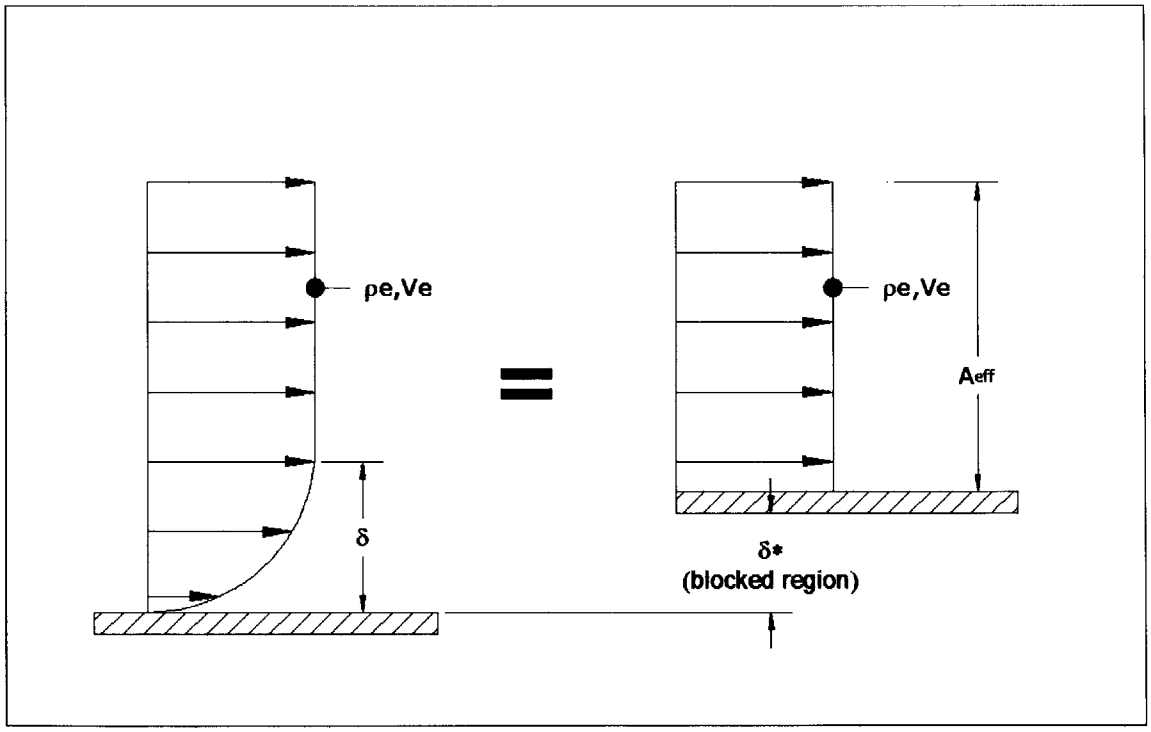

Figure 3.5: non-uniform flow represented by an equivalent stream at a reduced area.

Blockage is defined as the ratio of the blocked area ($A-A_{eff}$) to the total area and is computed as: $B = 1 - A_{eff}/A_{total}$. In this section it is however preferred to treat effective area as the metric for assessing the effect of flows with regions of non-uniform velocity.

In figure 3.5, the reduction in area per unit width from the actual flow to the equivalent uniform stream is known as the displacement thickness and it represents the amount of blocked area due to velocity retardation. Thus the displacement thickness is given as:

$$\delta^* = \int_0^{\delta} \left(1 - \frac{\rho V}{\rho_e V_e}\right) dy \tag{3.9}$$

In a three dimensional flow, the summation over the entire width of the displacement thickness of a stream in a plane constitutes the total blocked area at that plane (see Fig 3.6):

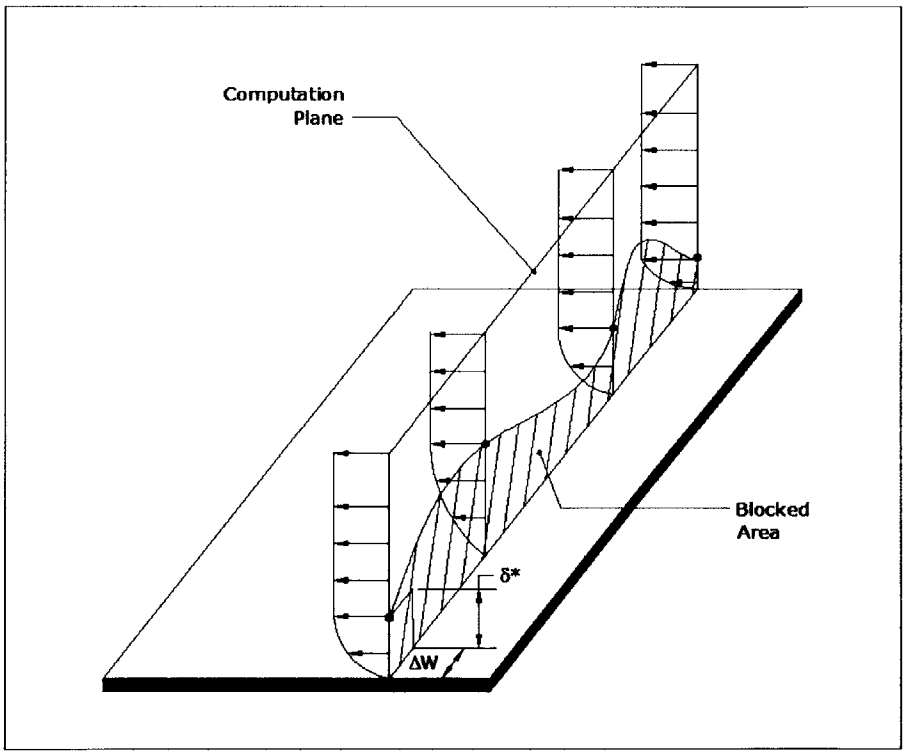

$$A_{blocked} = \sum \delta^* \cdot \Delta W$$

Figure 3.6 Representation of blocked area in a cross sectional plane.

For a centrifugal compressor, regions of non-uniform velocity are not only confined to the effects of boundary layers. Mixing due to the presence of wakes or secondary flows can also result into an effective flow area reduction.

Khalid [22] developed a methodology to compute the reduction in effective area due to the presence of endwall /tip clearance flows in an axial compressor. Shum [18] modified Khalid's model for its use in centrifugal compressors. For many flow situations in centrifugal compressors, Khalid/Shum method are not quite appropriate in quantifying the reduction of effective area of the flow in a centrifugal compressor. Murray [25] developed an alternative method for the estimation of the changes in the effective area between two centrifugal compressors. In the following, both methodologies are compared. The most suitable method in the evaluation of the reduced area for the current articles of research is determined. A brief explanation of the blockage effect is offered along with the description of the application of the two methods. Finally the obtained results are presented.

Khalid departs from a simple one dimensional velocity profile in an axial channel having a core region with high speed and two boundary layers, one at the hub and one at the casing. If the edges marking the division of the core from the boundary layers are known, then the limits of integration of e.q. 3.9 can be taken and δ^* can be computed for that particular profile. Depending upon the type of design , the magnitude of velocity on an axial compressor is usually non-uniform even within the core region. Since it is the velocity within the channel that is the quantity of interest, relative velocities W in a centrifugal compressor must be employed. The following figure (Fig. 3.7) shows the relative velocity profile at a location close to the pressure surface and at the exit of an impeller channel of the Production compressor.

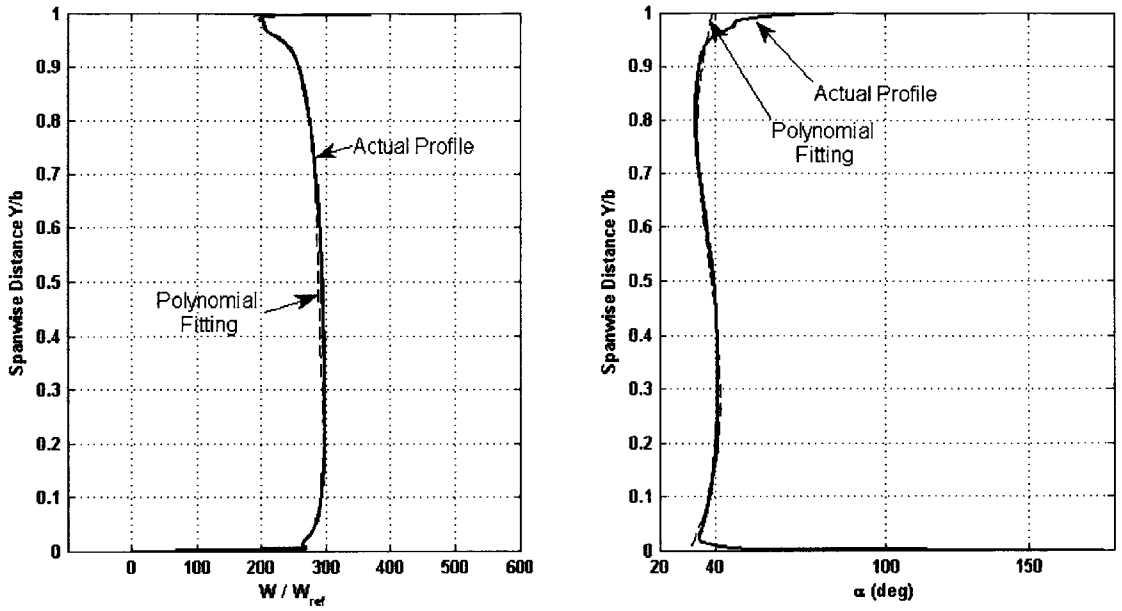

Figure 3.7: Relative velocity profile (magnitude and angle) of a region close to the pressure surface of an impeller blade. Solid line represents the actual profile and dashed line represents polynomial fitting.

The portions where speed is significantly lower constitute a distortion from the velocity of the mainstream and are designated as defect regions. Khalid [22] quantifies the level of distortion by computing the angle of deviation from the main flow direction (α) (i.e. radial direction for the exit of a centrifugal impeller). Angle distribution is also shown at Figure 3.7. The presence of a wake in the suction portion of the channel (jet-wake model) introduces cross flow that leads to additional distortion. The identification of a core region with a defined direction must thus be done in zones free from wakes. The following figure shows velocity and angle distributions at a location close to the suction surface where the effects of the wake are clearly seen:

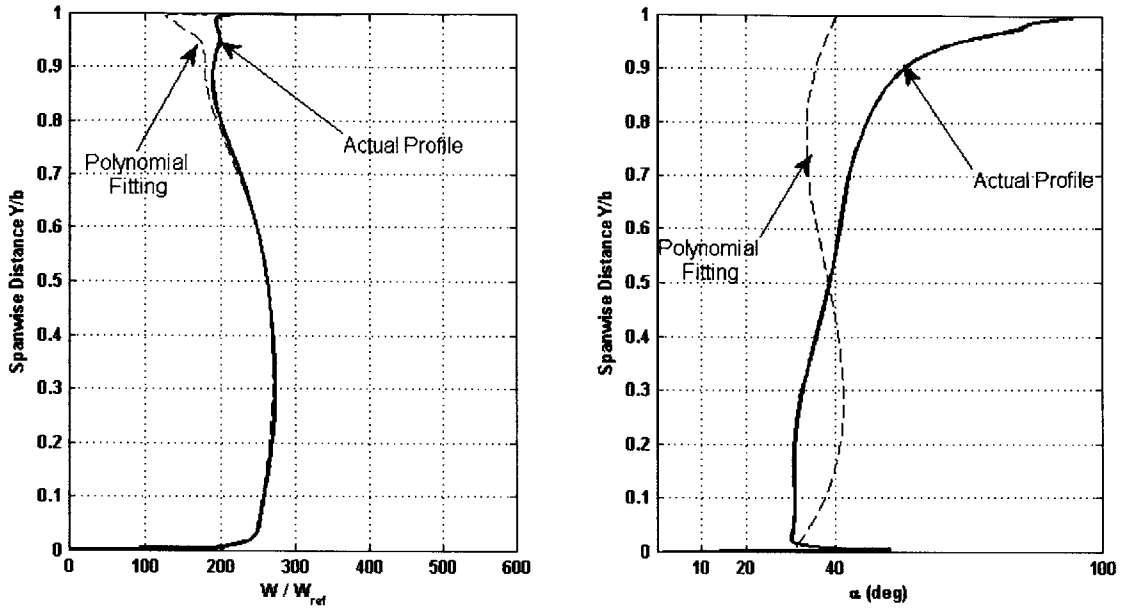

Figure 3.8 **Relative velocity profile (magnitude and angle) of a region close to the suction surface of an impeller blade. Solid line represents the actual profile and dashed line represents polynomial fitting.**

The next step is the definition of the edges of the distortion. If a core region is recognized, the values of the flow angle and speed can be extrapolated to those portions where the distortion is located. Then the velocity at the defect region is projected over the main flow direction (Vm) to assess the level of distortion. A dashed line in Figure 3.7 shows the extrapolation obtained by third order polynomial fitting of velocity magnitude and angle. Despite the fact that core velocity is not uniform within the core, its variation is not as pronounced as in the defect regions. Khalid thus proposes the computation of the gradient in velocity magnitude $\nabla_{r,\theta}|Vm|$ for the identification of the edges of the defect regions. Shum's[18] adaptation of Khalid's method, defines the edges of the distortion as those points where the gradient of the velocity normalized by the net momentum over the impeller diameter is above 2.5 (cutoff value):

$$\frac{|\nabla_{r,\theta} W_m|}{(\rho W)_{ave}/D} > 2.5$$

When isolated regions of low velocity gradients are visualized within what has been recognized as distorted regions, Khalid's procedure contemplates the alteration of the value of velocity in such locations so as to make them part of the distortion. Figure 3.9a shows cutoff contours of Khalid's axial passage clearly indicating that the regions contributing to flow blockage are confined to the endwalls of the passage. Murray [25] found that due to the complex jet and wake flow at the exit of the impeller, the application of Khalid's method was somewhat not practical for his compressors and developed an alternative method. Figure 3.9b and 3.9c show cutoff value contours at the exit of the Production and Enhanced impeller at a similar instant in time for MASS1. The regions enclosed by the contours are regions of "unblocked area" where cutoff values are less than 2.5. It is clear from the figure that areas of velocity retardation are not only confined to regions close to the walls of the passage and the use of Murray's method over Khalid/Shum is thus adopted.

The method developed by Murray is not an accurate computation of the effective area but is a good approach in quantifying the changes in the flow blockage from one compressor to another. It relies on the assumption that the mass flow that is aligned with the mean velocity direction is the only mass that flows through an area that is unblocked. It does not make use of any modifications to the velocity profile at any location. The change in effective area may be computed as:

$$\Delta A_{eff} = \Delta\left(\frac{\dot{m}\int d\dot{m}}{\int \rho W_{TF} d\dot{m}}\right) \tag{3.10}$$

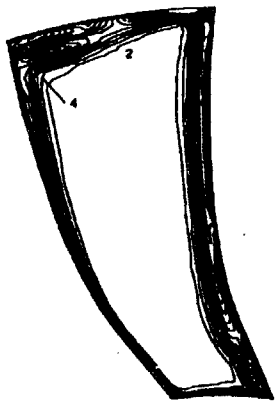

a) Khalid's Axial Passage

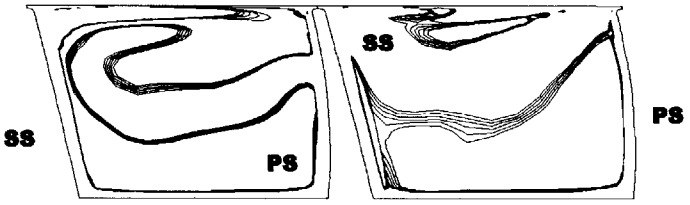

b) Production

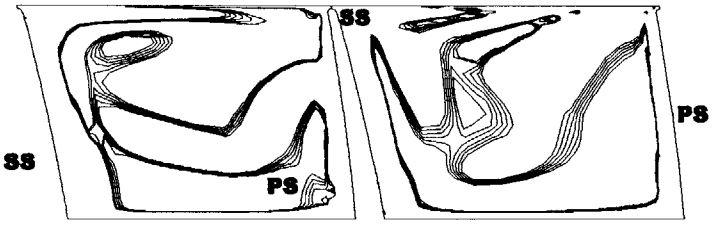

c) Enhanced

Figure 3.9: Contours of relative velocity gradients in the normal and bi-normal direction of the flow showing distortion regions: a) Khalid [22], b) Production and c) Enhanced

The obtained results from Murray's method are shown in the table below. Values of area are normalized by a reference value.

	A_{eff} / A_{ref}		$\frac{\Delta A_{eff}}{A_{effprod}}$	$\frac{(\%)\Delta A_{eff}}{A_{effprod}}$
	Production	**Enhanced**		
MASS1	1.00	1.03	0.0314	3.14
MASS2	0.97	1.02	0.0436	4.36

Table 3.3: Change in effective area between compressors computed by Murray's method [23]

It is inferred from these results that the Enhanced compressor has higher effective flow area. In Shum's model, higher effective area will produce higher values of pressure and so this is the trend shown for the Enhanced compressor.

Although losses are higher for the Enhanced compressor, their detrimental effect on the pressure ratio is surpassed by the favorable effect of the increase in the effective flow area (changes in effective area are one order of magnitude higher than the losses, see table 3.2 and 3.3). One possible reason behind these observations is the connection between the sources of loss, i.e. tip leakage flow, and the improved effective area, details on this can be found in Shum [18].

3.5 STAGE EFFICIENCY.

A closing step in the analysis of the time-average performance of the compressors, is the evaluation of the impeller and the stage efficiency. Efficiency is computed from the appropriately averaged stagnation quantities (section 2.4) and the expression for efficiency:

$$\eta = \frac{W_{ideal}}{W_{real}} = \frac{\prod_t^{\frac{\gamma}{\gamma-1}} - 1}{\tau_a - 1} \tag{3.11}$$

Normalized results are shown in the table below:

		Adiabatic Efficiency: η / η_{pmass1}		
		Production	Enhanced	%Δ
Stage	MASS1	100.0	100.52	0.52
	MASS2	102.4	100.99	-1.41
Impeller	MASS1	100.0	99.00	-1.00
	MASS2	99.8	99.47	-0.35

Table 3.4: Time averaged stage and impeller adiabatic efficiency of Production and Enhanced compressor.

The Enhanced compressor shows a lower efficiency for the impeller than the Production compressor at both points of operation. The entropy generation due to tip leakage is stronger in the Enhanced compressor because of stronger Impeller-Diffuser interaction and stronger leakage flow. Overall stage efficiency is higher in the Enhanced compressor operating at MASS1 but lower at MASS2 (see Figure 3.10) This shows that the flow in the diffuser features as an additional source of loss that is dependent upon the point of operation. It is suggested that the change in the flow matching between the modified impeller of the Enhanced design and the diffuser at that specific point of operation could possibly be the source of the observed difference in performance from the production design.

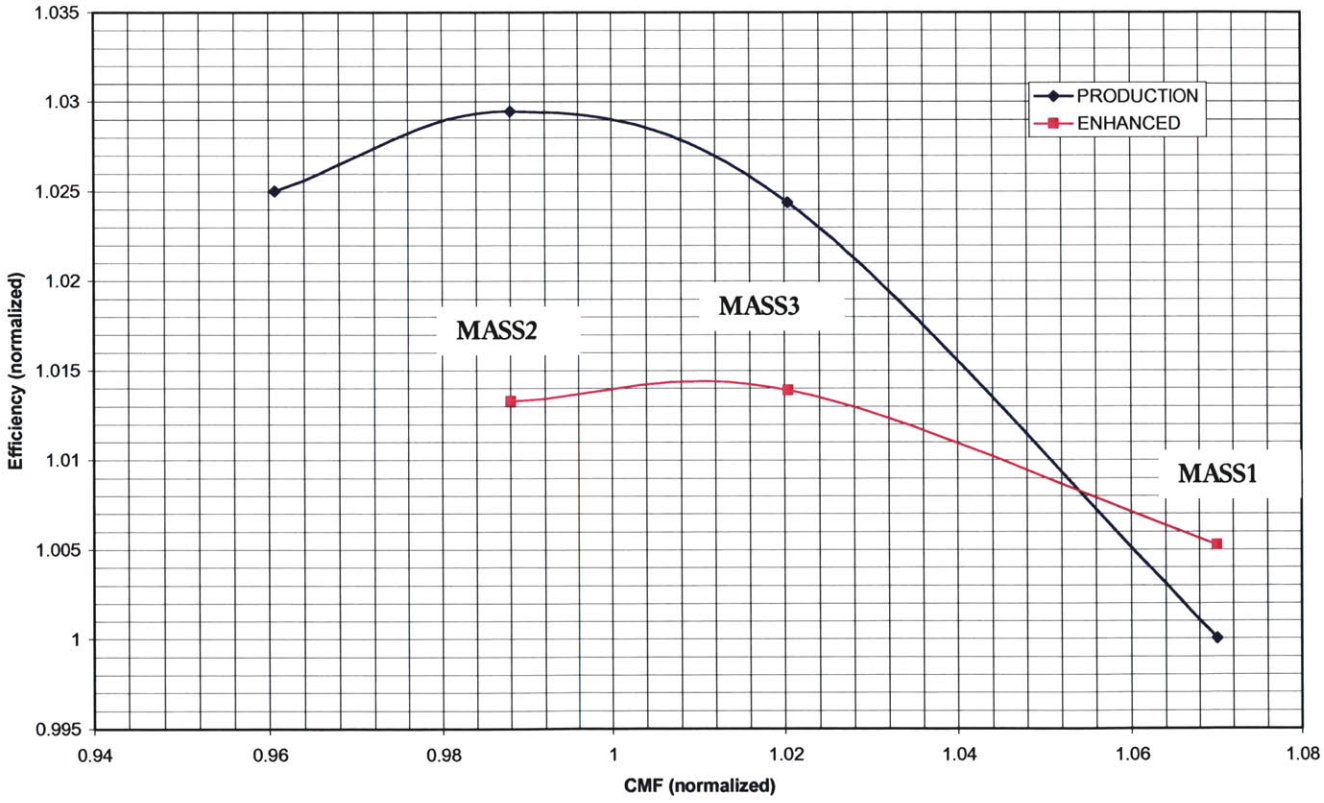

Figure 3.10: Efficiency curves. Note values are normalized by reference quantities no necessarily in coincidence with those in Figue 3.1

3.6 SUMMARY

From the results obtained by TURBO, the Enhanced compressor presents an overall increase in time-averaged pressure ratio (total and static) of nearly 3%.

The data in this chapter also demonstrates that the increase in static pressure ratio from the impeller of one compressor to another involves rather more complicated flow mechanisms than a simple increase in impeller radius. The losses resulting from the stronger impeller-diffuser interaction of the Enhanced compressor have an adverse impact on pressure ratio. However tip leakage flow, which is the mechanism through which most of the losses are generated, has a positive influence in the blockage of the flow at the impeller. This last effect has proven to be the dominant cause in the increase of static pressure ratio between the two compressors.

The larger change in stage efficiency of the Production compressor with respect to the Enhanced when moving from operation point of MASS1 to MASS2, suggests that the losses occurring in the diffuser are dependent on the point of operation and could be related to the flow matching between the impeller and the diffuser.

CHAPTER 4

The Unsteady Flow Field

4.1 INTRODUCTION

In any vibrational phenomenon, the forced response of the oscillatory system depends to a large extent on the nature of the forcing function. In chapter 3, differences in the pressure field between the two compressors were established on a time-averaged basis without any further insight of time variation and spatial distribution of the pressure field acting on the blades. Resonant behavior will likely occur when the frequency of the unsteady loading and its spatial distribution are coincident with the natural mode frequency and mode shape of the blade structure. Thus the study of the unsteady behavior of the flow field is of importance.

The theme of this chapter is to characterize the unsteady loading of the impeller blades followed by a delineation of the main differences of this quantity between the Enhanced and the Production compressor. Unsteady computational results are presented to elucidate how the pressure distribution in the vicinity of the diffuser vane leading edge and the impeller diffuser relative motion go toward setting the unsteady and spatial extent of the loading in the impeller blades.

The results are employed to answer the hypothesis originally formulated by Smythe [17] which relates the incidence angle to the behavior of the pressure field at the exit of the impeller. The correlation of the incidence angle to the levels of loading has been previously examined in similar studies such as that by Rabe and Kenyon [15] who analyzed the shock structure and the loading on the blades of a transonic fan.

4.2 CHARACTERIZATION OF BLADE LOADING

Previous work performed by Smythe [17] on both compressors, revealed key features about the steady and unsteady loading of the impeller blades. Smythe found that the meridional distribution showed a different pattern from one case to another with the level of loading being higher for the Enhanced compressor. It was also noted that the peak values of loading varied with spanwise location on each compressor, with the highest values usually present in the hub region. This section broadens the analysis performed by Smythe by focusing on the evolution of loading with time. The attempt is to establish the differences in peak values of loading from one compressor to another and to characterize the meridional distribution of this quantity.

4.2.1 Time-averaged loading of Production and Enhanced Compressor.

A first examination is taken into time-averaged loading. Figure 4.1 shows time-averaged loading as a function of meridional distance at a mid-span location in the impeller main blade and splitter. Both compressors are represented at different points of operation (MASS1, MASS3 and MASS2 see Figure 3.1). MASS1 consists of an operating point close to design, MASS2 to a point close to stall and MASS3 has been chosen to be approximately in between these two. Differences in the loading pattern for the main blade do not seem to be significant from one compressor to another. In the splitter blade however, these differences are finite in a region of 15% chord-wise distance taken from the trailing edge, with higher values for both compressors at MASS2 operation. The aeromechanic difficulty was encountered in the splitter blade of the Enhanced compressor. From the plots, the Production compressor has slightly higher loading distribution than the Enhanced. This is not necessarily in contradiction with the fact that the Enhanced compressor has higher pressure ratio than the Production since the distribution is only taken along a meridional distance at mid-span.

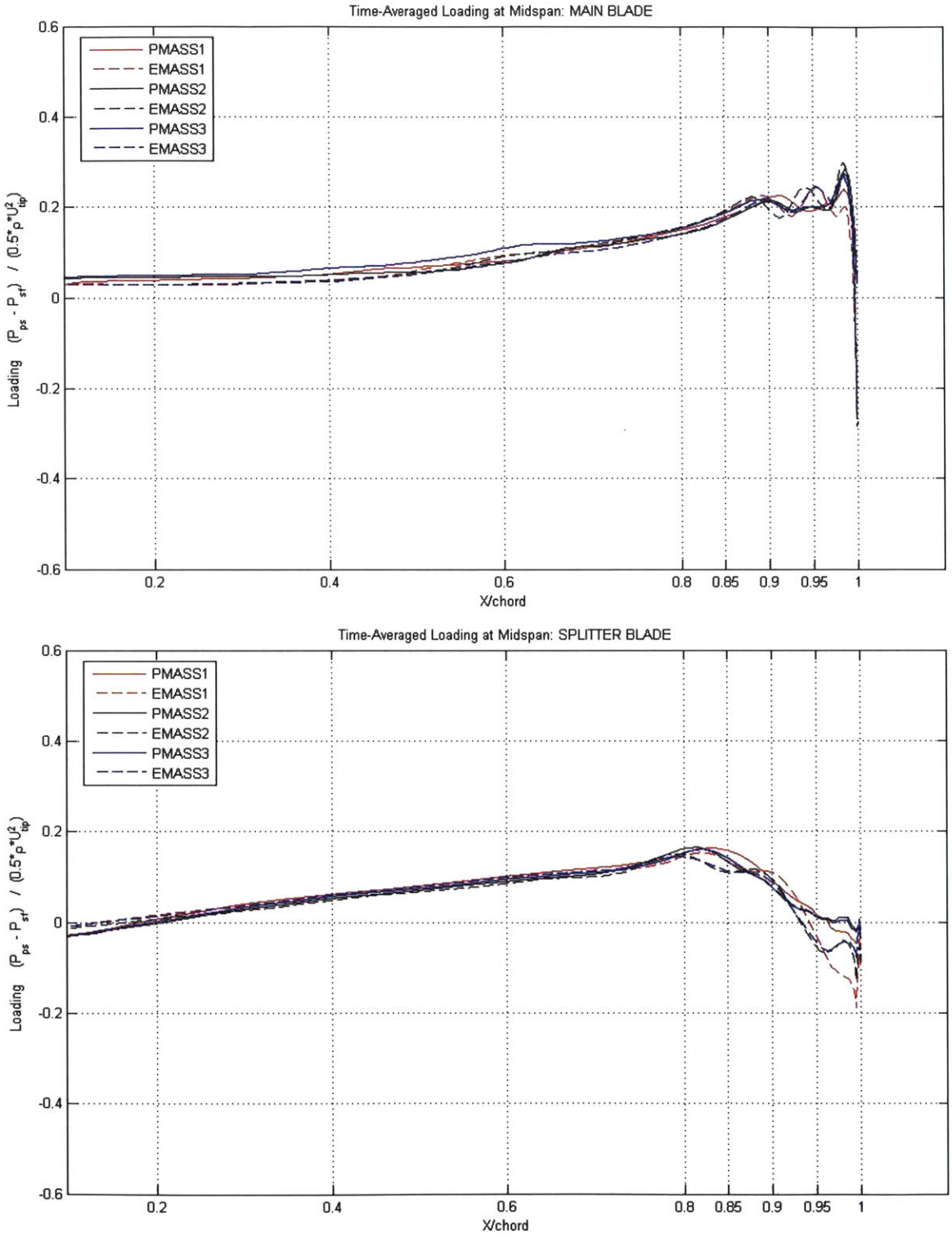

Figure 4.1: Meridional distribution of time-averaged loading at mid-span. Main blade and Splitter. (meridional distance normalized by the main blade and splitter chord accordingly). Curves shown for Production (P) or Enhanced (E) compressors at different operating points (MASS1, MASS2, MASS3)

4.2.2 Unsteady Loading

As described in section 2.3, the unsteady behavior of the flow field in turbomachinery passages is primarily defined by the interaction of a blade row with its adjacent row [9,10,23]. Unsteady impeller blade loading is a cyclic quantity that repeats with the frequency of the passing vanes of the diffuser as seen by the impeller. This is the situation for synchronous excitation. However for asynchronous excitation, the frequency need not to be that of the passing vanes. Measurements of loading for both compressors are taken at time instants spaced by 1/8 of the diffuser vane passing period at identical positions with respect to the diffuser vanes. Spacing of 1/8 of the diffuser vane passing period is chosen in the analysis throughout this chapter because the ratio of the vane passing period of the impeller to that of the diffuser is a multiple of 1/8 and thus permits one to visualize events at same relative positions when seen either from the impeller or from the diffuser. The obtained results are shown for three span-wise locations: hub (10%spanwise), mid-span (50%) and tip (90%) (Figure 4.2). Several features are identified:

- In both compressors the loading patterns are similar from hub to mid-span, but differ greatly at the tip (see Figure 1.1). The highest amplitudes are present at the hub.

- The unsteady behavior of loading for the main blade is localized in a region ranging from 80% to 100% chordwise. The region of unsteadiness extends further into the blade as the meriodinal location is closer to the tip of the blade. In the splitter blade, unsteadiness covers a larger portion of the chord because the chord is smaller and the values range from 60% to 100% of the splitter chord. However the extent of unsteadiness is the same in spatial units for both blades(or ~80% to 100% in terms of the main blade chord).

- Peak to peak magnitude in loading is higher for the Enhanced compressor than for the Production. Also, loading values of the splitter are not different than those from the main blade at hub or mid-span locations but differ at the tip from those of the

main blade at the same location (tip). The greatest amplitudes are registered for operation at MASS2.

- The variation of the loading distribution with time attenuates as it propagates upstream of the impeller trailing edge. For the Production case, the loading unsteadiness decays faster than for the Enhanced. This can be appreciated by the extension of the envelopes bounding the loading (see Figure 4.2).

- The maximum amplitude of loading at all mid-span locations occurs at 3/8 of the diffuser passing period in the main blade, and at 6/8 in the splitter blade.

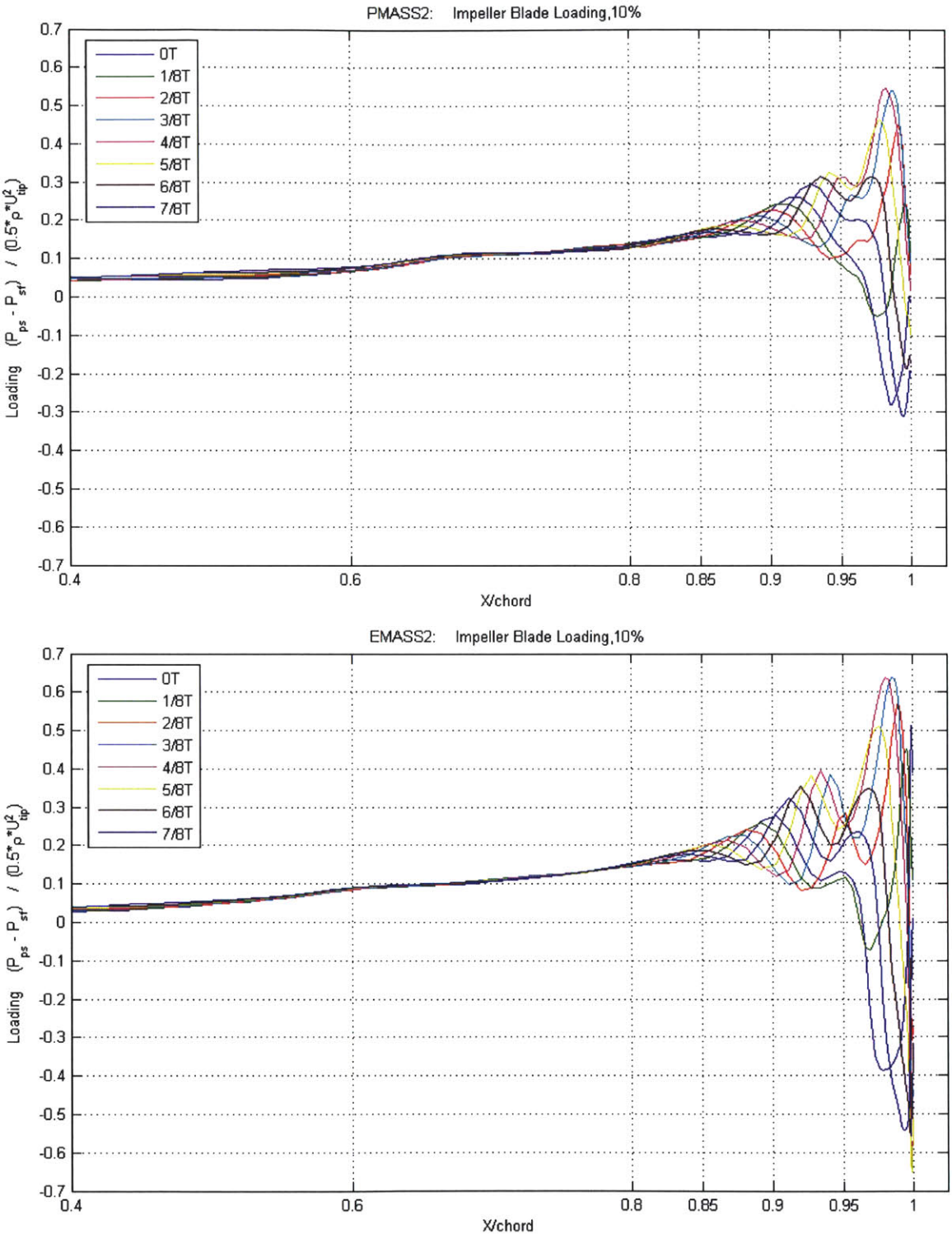

Figure 4.2a: Meridional distribution of loading at different time instants at MASS2. 10% spanwiselocation (hub). Enhanced (EMASS2) and Production (PMASS2) compressor (main blade: meridional distance normalized by the main blade chord)

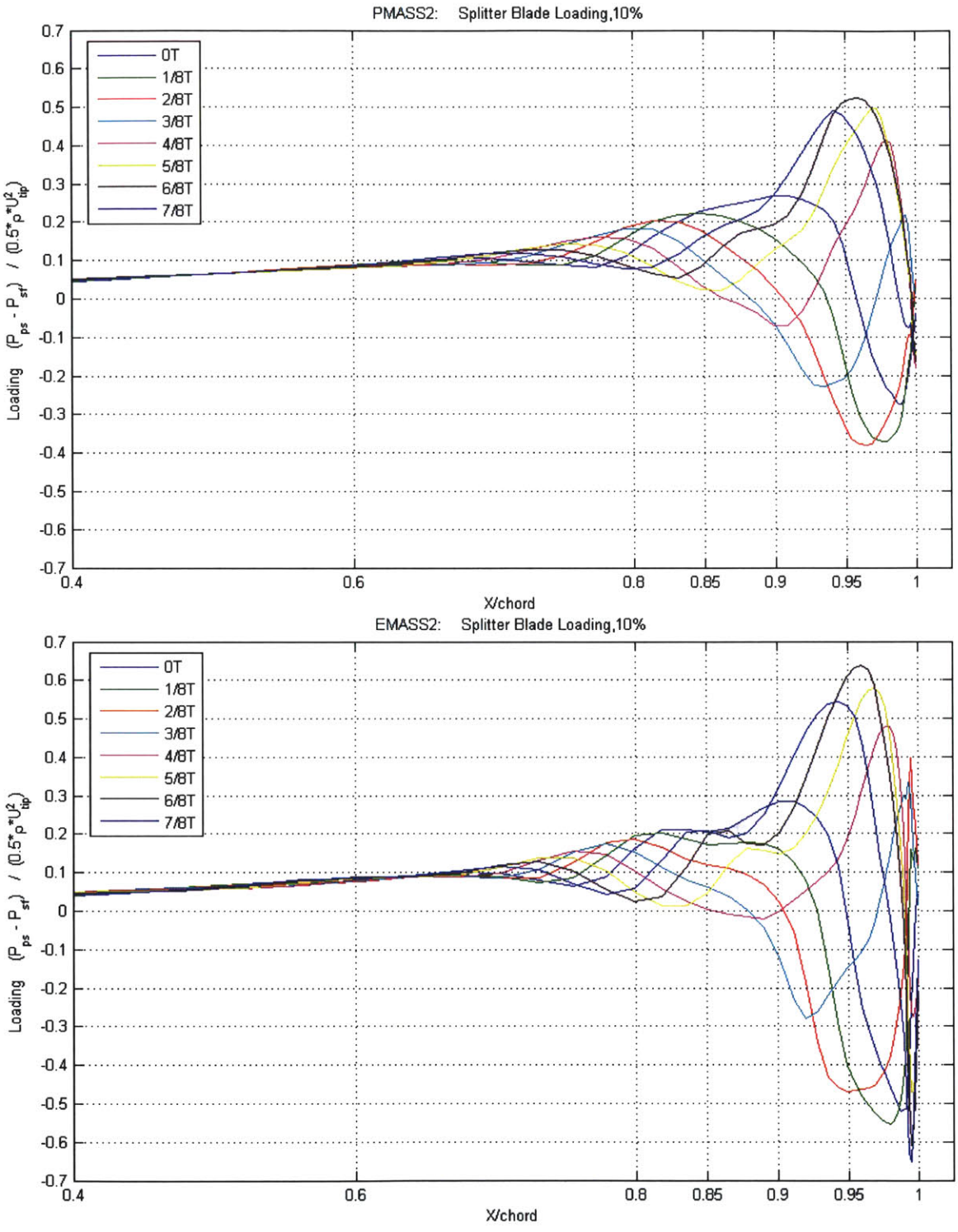

Figure 4.2b: Meridional distribution of loading at different time instants at MASS2. 10% spanwiselocation (hub). Enhanced (EMASS2) and Production (PMASS2) compressor (splitter blade: meridional distance normalized by splitter chord)

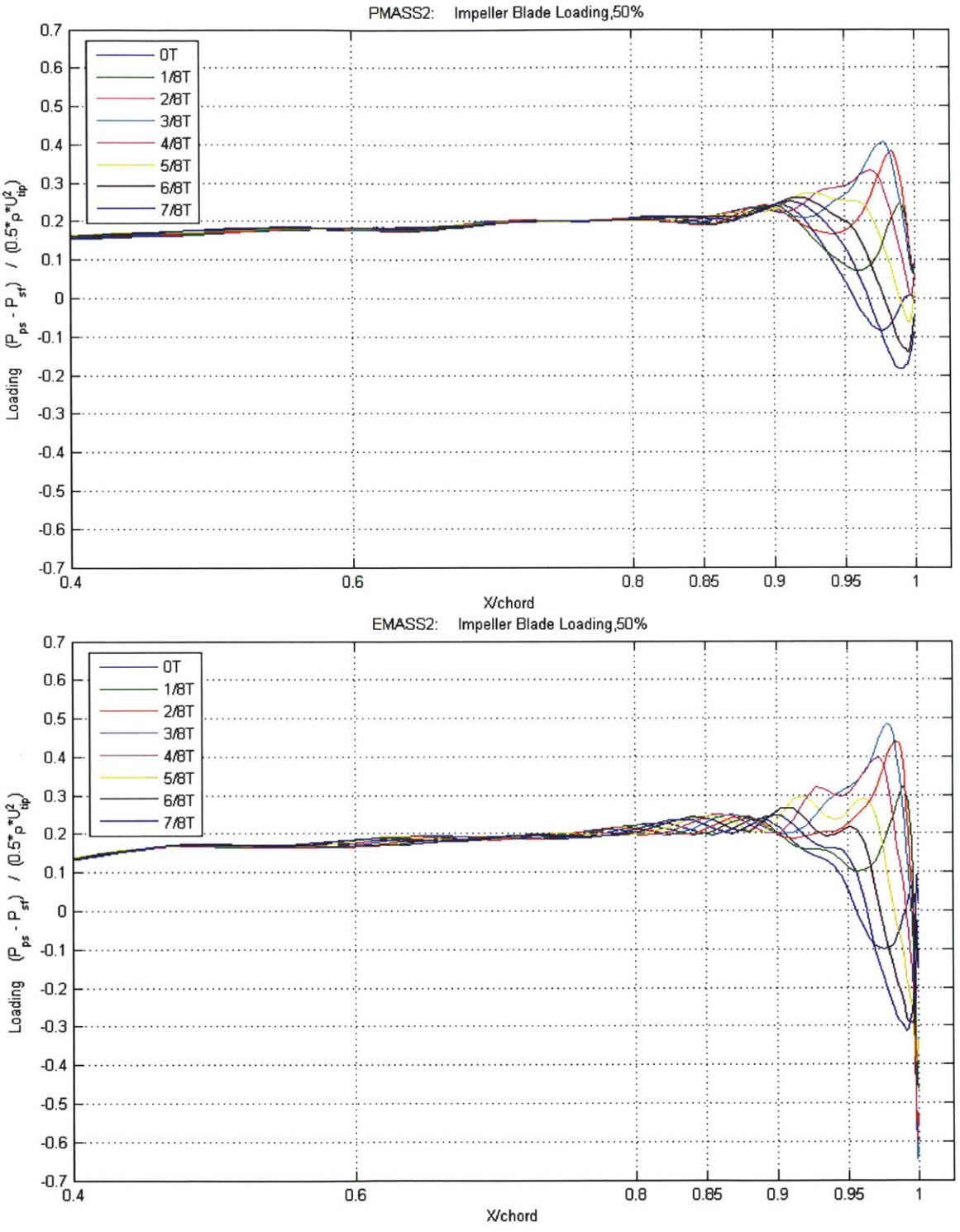

Figure 4.2c: Meridional distribution of loading at different time instants at MASS2. 50% spanwise location (mid-span). Enhanced (EMASS2) and Production (PMASS2) compressor (main blade: meridional distance normalized by the main blade chord)

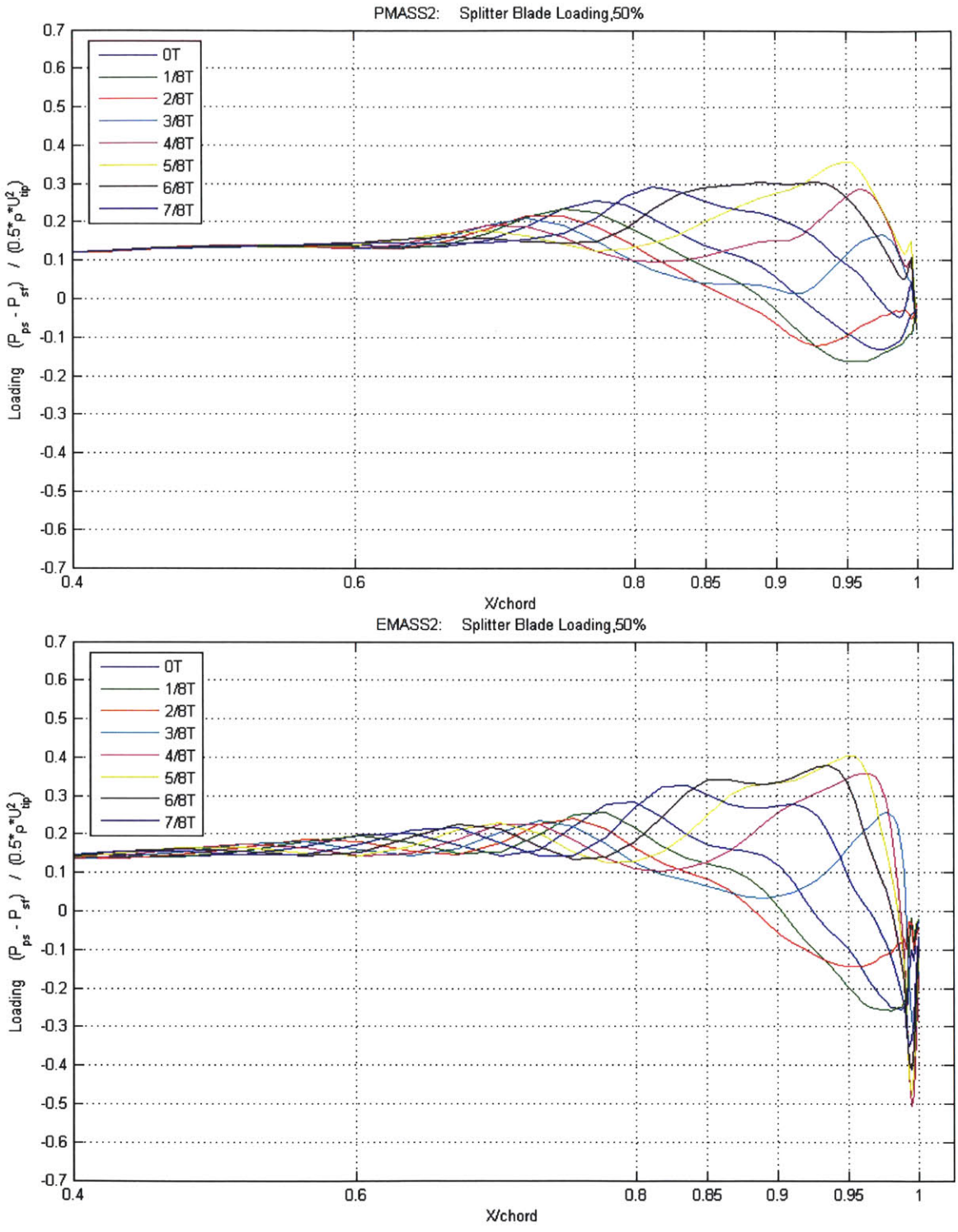

Figure 4.2d: Meridional distribution of loading at different time instants at MASS2. 50% spanwise location (mid-span). Enhanced (EMASS2) and Production (PMASS2) compressor (splitter blade: meridional distance normalized by splitter chord)

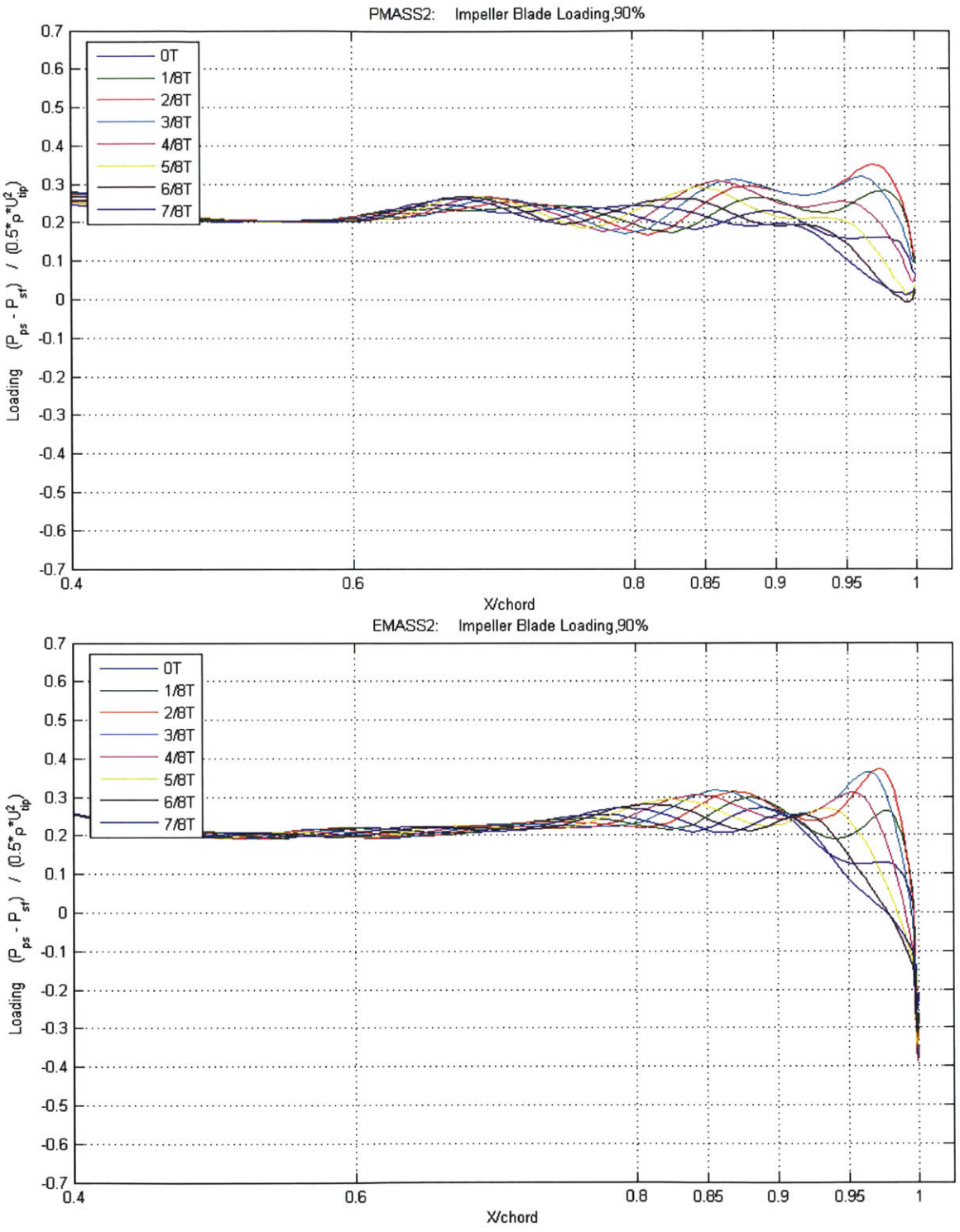

Figure 4.2e: Meridional distribution of loading at different time instants at MASS2. 90% spanwise location (tip). Enhanced (EMASS2) and Production (PMASS2) compressor (main blade: meridional distance normalized by the main blade chord)

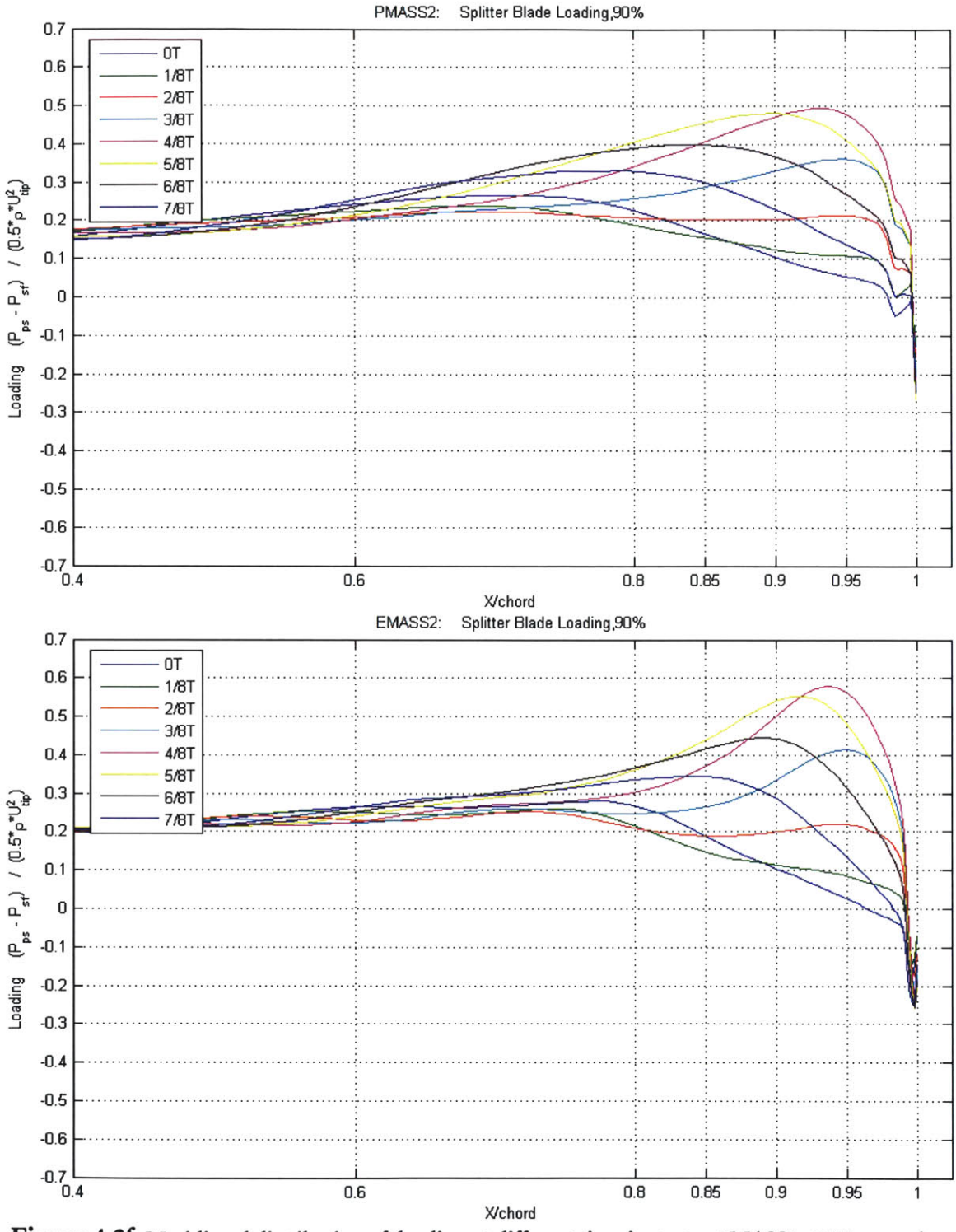

Figure 4.2f: Meridional distribution of loading at different time instants at MASS2. 90% spanwise location (tip). Enhanced (EMASS2) and Production (PMASS2) compressor (splitter blade: meridional distance normalized by splitter chord)

Tables 4.1a and 4.1b summarize some of the most important features in loading distribution of the two compressor blades. These features are graphically shown in Figure 4.3:

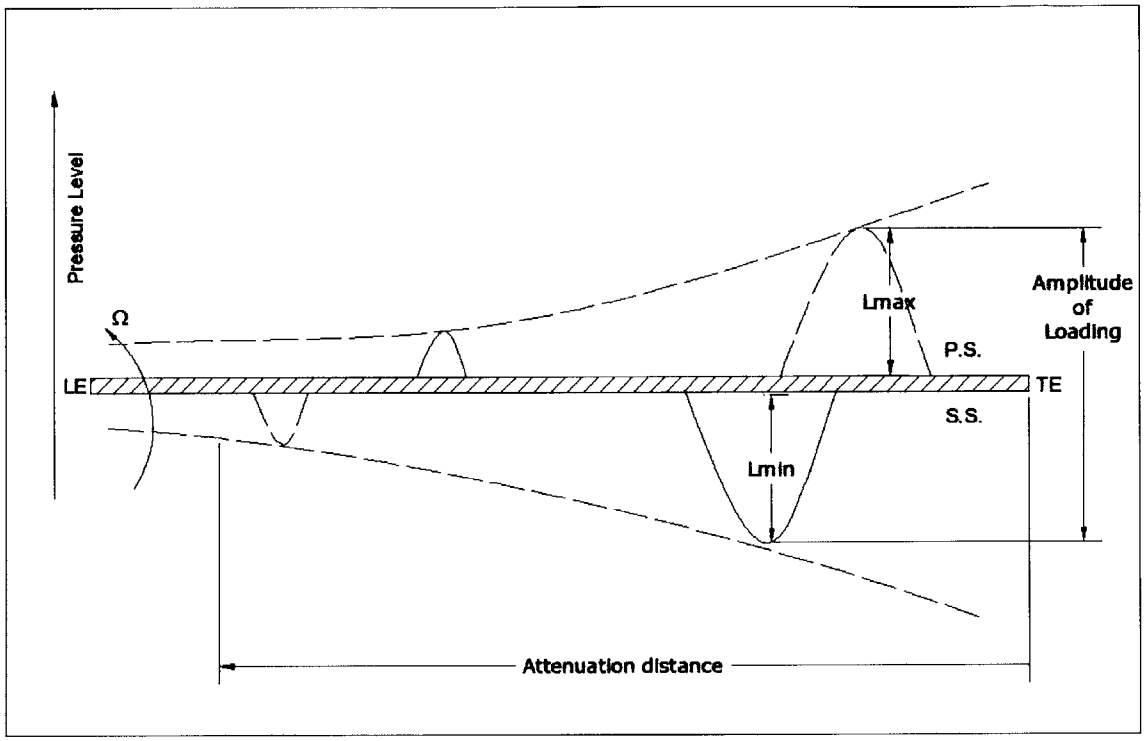

Figure 4.3: Features of interest in loading

From the tables the amplitude of loading in the main blade of the Enhanced compressor is ~1.8 times larger than for the Production. For the splitter blade the Enhanced compressor is ~1.4 times larger. From testing data, the Enhanced compressor presented a strain being twice as large as the one of the Production as reported in [21].

	MASS1						
	Production			Enhanced			$\frac{\Delta enhan}{\Delta prod}$
	MAX	MIN	Δ (amplitud of loading)	MAX	MIN	Δ (amplitud of loading)	
HUB	0.517	-0.186	0.703	0.561	-0.568	1.129	1.61
MID	0.347	-0.138	0.484	0.374	-0.563	0.937	1.94
TIP	0.427	0.001	0.426	0.420	-0.374	0.794	1.86
						Average	**1.80**

	MASS3						
	Production			Enhanced			$\frac{\Delta enhan}{\Delta prod}$
	MAX	MIN	Δ (amplitud of loading)	MAX	MIN	Δ (amplitud of loading)	
HUB	0.526	-0.259	0.784	0.603	-0.587	1.190	1.52
MID	0.374	-0.162	0.535	0.438	-0.479	0.917	1.71
TIP	0.388	0.007	0.381	0.360	-0.376	0.736	1.93
						Average	**1.72**

	MASS2						
	Production			Enhanced			$\frac{\Delta enhan}{\Delta prod}$
	MAX	MIN	Δ (amplitud of loading)	MAX	MIN	Δ (amplitud of loading)	
HUB	0.546	-0.310	0.856	0.638	-0.652	1.290	1.51
MID	0.405	-0.183	0.588	0.486	-0.646	1.132	1.92
TIP	0.396	-0.007	0.404	0.437	-0.388	0.825	2.04
						Average	**1.82**

Table 4.1a: Summary of important features of loading . (Main blade, normalized Values)

	MASS1						
	Production			Enhanced			$\frac{\Delta enhan}{\Delta prod}$
	MAX	MIN	Δ (amplitud of loading)	MAX	MIN	Δ (amplitud of loading)	
HUB	0.470	-0.289	0.759	0.483	-0.498	0.980	1.29
MID	0.359	-0.098	0.457	0.389	-0.424	0.813	1.78
TIP	0.507	-0.276	0.783	0.618	-0.292	0.909	1.16
						Average	**1.41**

	MASS3						
	Production			Enhanced			$\frac{\Delta enhan}{\Delta prod}$
	MAX	MIN	Δ (amplitud of loading)	MAX	MIN	Δ (amplitud of loading)	
HUB	0.490	-0.339	0.828	0.561	-0.573	1.134	1.37
MID	0.356	-0.121	0.477	0.396	-0.325	0.721	1.51
TIP	0.496	-0.275	0.771	0.571	-0.281	0.852	1.11
						Average	**1.33**

	MASS2						
	Production			Enhanced			$\frac{\Delta enhan}{\Delta prod}$
	MAX	MIN	Δ (amplitud of loading)	MAX	MIN	Δ (amplitud of loading)	
HUB	0.5250	-0.3822	0.9071	0.6377	-0.6526	1.2903	1.4224
MID	0.3566	-0.1622	0.5188	0.4039	-0.5076	0.9115	1.7570
TIP	0.4946	-0.2654	0.7600	0.5791	-0.2586	0.8377	1.1022
						Average	**1.43**

Table 4.1b: Summary of important features of loading. (Splitter blade, normalized values)

4.2.3 The effect of diffusion on loading structure.

The overall level of loading on a blade can be expressed in terms of relative velocities through the de-Haller number. The de-Haller number is defined as the ratio of the exit relative velocity to the inlet relative velocity: W_2/W_1. In his study, Gould [26] showed that de-Haller number decreases with increasing corrected mass flow and that this results in an increase in the extent of the region of unsteadiness on the impeller blade. Figure 4.4 plots the extent of unsteadiness as a function of de-Haller number (low de-Haller represents high loading). Note that the extent of unsteadiness is measured in terms of a percentage of the impeller main blade chord from the leading edge of the impeller.

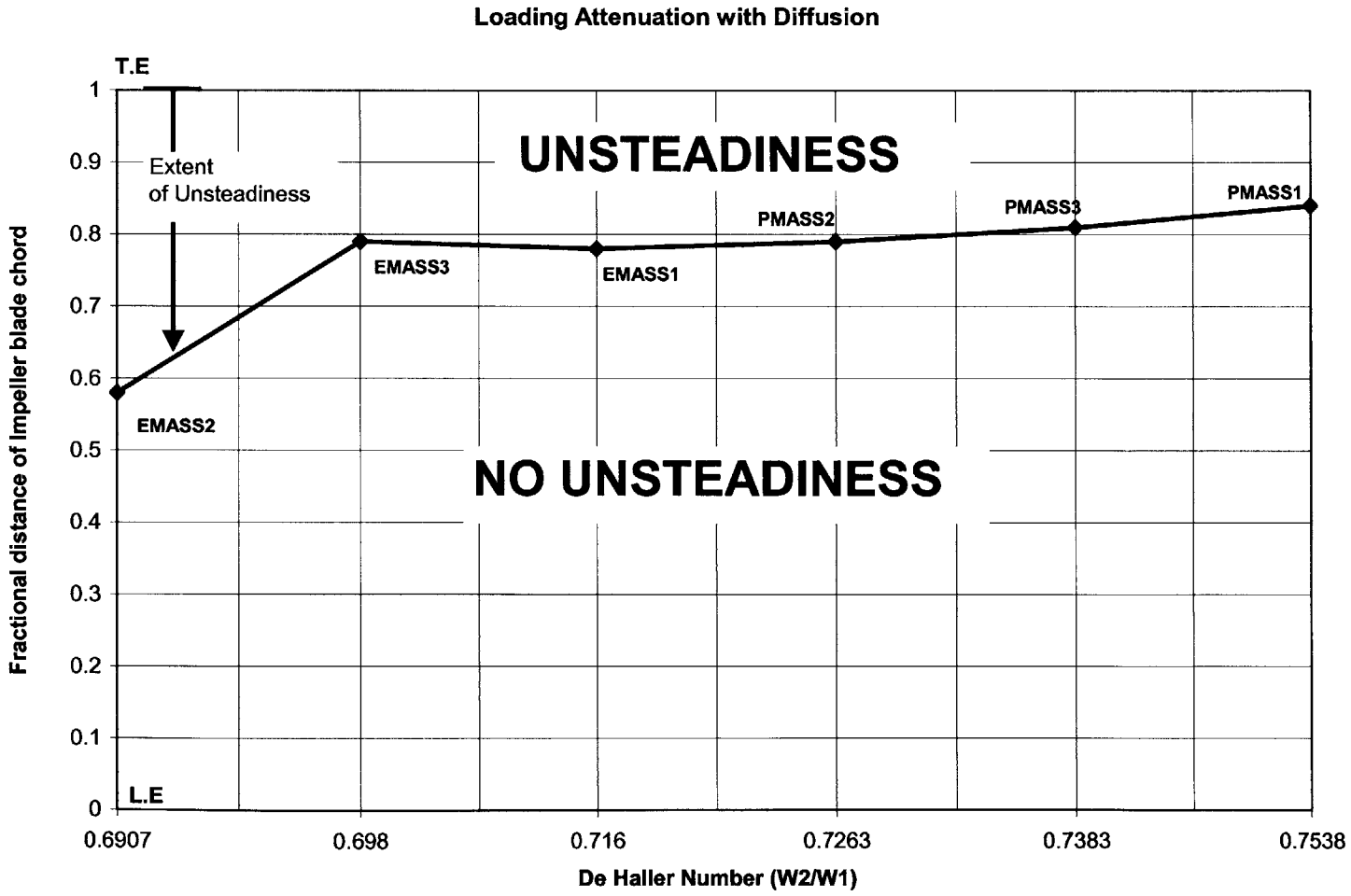

Figure 4.4: Extent of unsteady loading vs de-Haller number

As shown in the figure, the lowest de-Haller numbers are registered for the Enhanced compressor at the three points of operation. Large diffusion (low de-Haller) will have higher penetration than lower diffusion (high de-Haller) and thus attenuation will be reduced. These results are in accord with the observations made by Gould [26].

4.3 PRESSURE WAVE STRUCTURE

Differences in the loading pattern of the impeller blades have been established between the two compressors. An understanding of loading and its nature is a necessary requirement in the assessment of the perceived aeromechanic difficulty. Important features of the flow field leading to the formation of unsteady loading are described in this section.

As shown by the results in section 4.2, the highest amplitudes of loading are obtained when operating at reduced mass flow. It is thus of interest to look at the features of the flowfield at MASS2 in the quantification of loading. The Production compressor is used as the baseline case for the following discussion. Although the Production and the Enhanced compressors have quantitatively different flow features, qualitatively they are the same so the examination of a single compressor suffices for this analysis.

In order to characterize loading, an impeller passage is followed as it completes one vane passing period of the diffuser. Pressure contours are displayed every 8^{th} of the period for a mid-span location at the exact time instants and relative positions of section 4.2.2 (Figure 4.5). The evolution of the pressure over the surfaces of the main impeller blade is followed. At time t=0T, the impeller blade (1) (see figure 4.5) approaches the zone of high pressure that surrounds the leading edge of the diffuser vane (2). As the blade moves closer, a region of high pressure (A) builds on the pressure surface of the impeller blade at the trailing edge (t=1/8T, 2/8T). This region propagates upstream into the impeller channel (t=3/8T, 4/8T) and begins to decay as it reaches distances further upstream (t=5/8T , 6/8T). At T=7/8 the pressure contours recover nearly the same shape and values as those at t=0T. The same process occurs at the suction surface of the blade but with a lag in time. The formation of the high pressure region (B) is not evident until time 4/8T and 5/8T and does not propagate to the same extent as that on the pressure surface of the impeller blade. By the time the pressure reaches a maximum on the pressure surface on the impeller blade trailing edge, it has a low value at the suction surface (3/8T, 4/8T), the effect being reversed for later times in the period (6/8T, 7/8T). During these times, high levels of loading should be expected. This is the trend shown by the loading distributions of Figure 4.2.

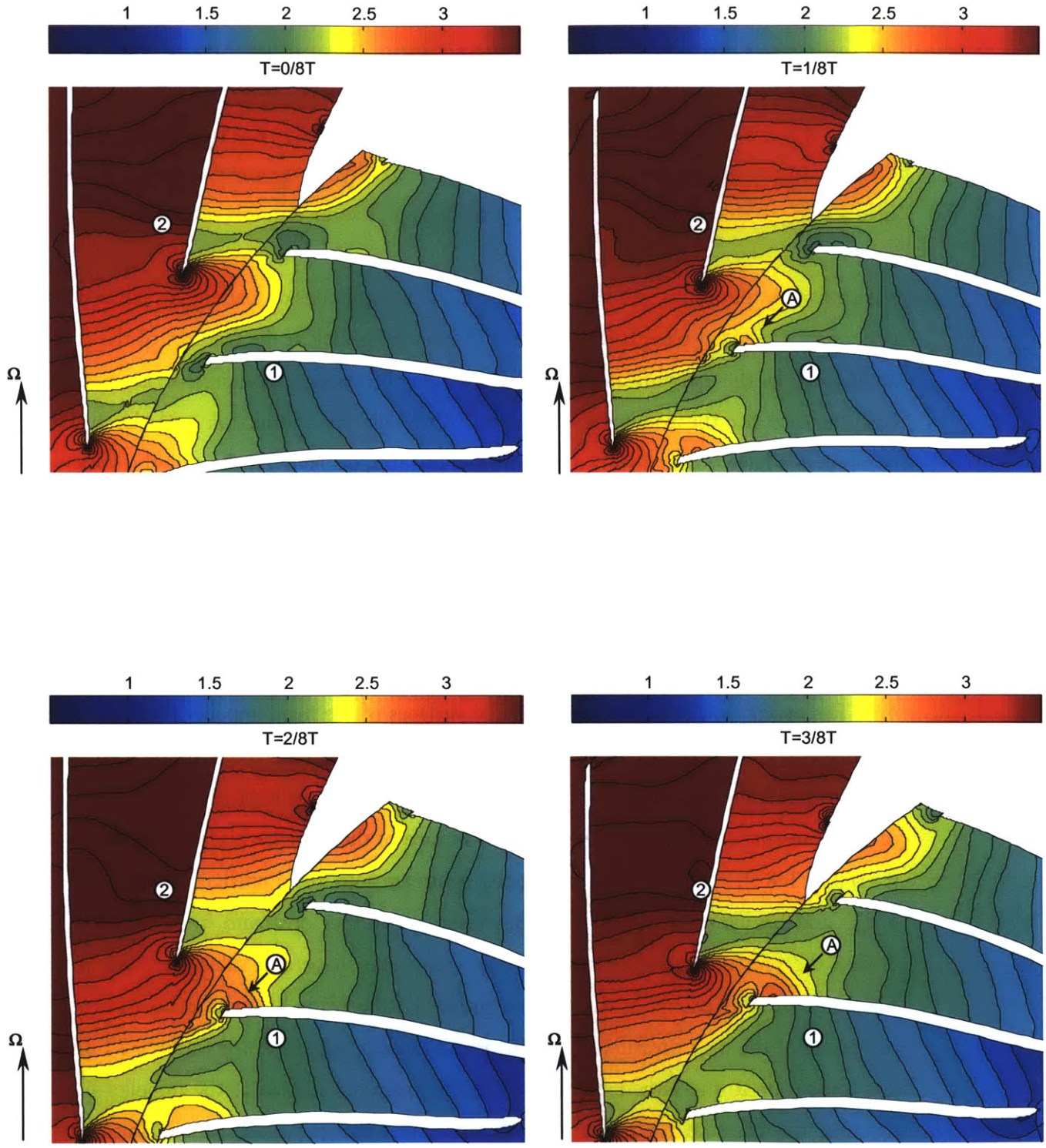

Figure 4.5a: Pressure development over impeller blade as a function of position (normalized).

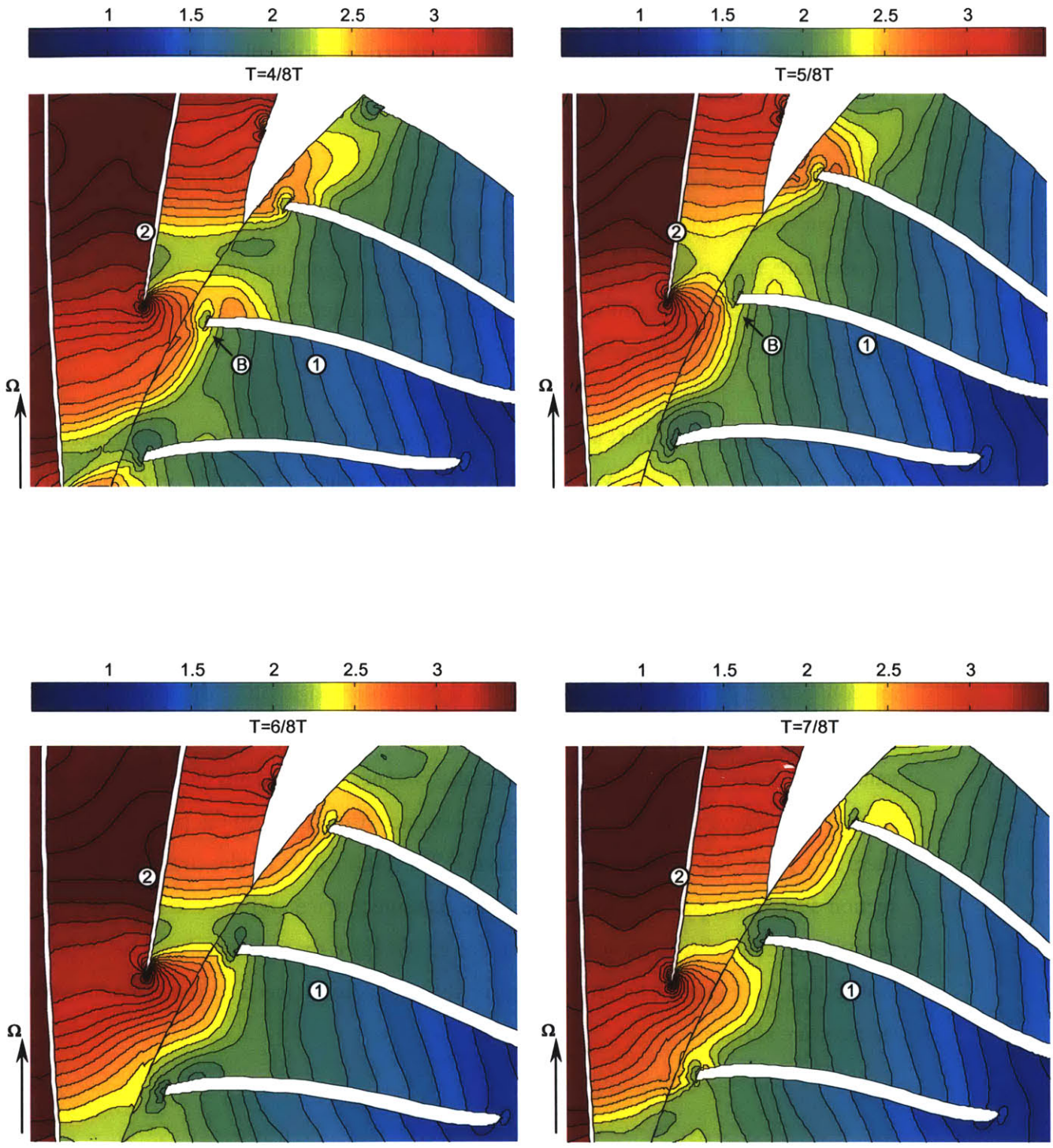

Figure 4.5b: Pressure development over impeller blade as a function of position (normalized).

From these observations, it is inferred that the level of pressure around the vanes of the diffuser is directly related to the level of loading acting on the blades of the impeller. Also the unsteady loading on the impeller blades is set by the vanes of the diffuser.

The regions of pressure acting over the surfaces of the impeller blade (A and B in Fig 4.5) are disturbances that propagate as pressure waves upstream and into the impeller channel. To illustrate this, plots of meridional distribution of pressure along the surfaces of the blades (pressure and suction) at different time instants over a vane passing period are shown in Figure 4.6 at 10% span-wise location.

The pressure surface exhibits a wave standing close to the trailing edge of the impeller blade at time 0/8T. At 2/8T, a new wave is formed at the trailing edge and is propagated into the channel. The peak value of the wave reaches a maximum at t=3/8T and begins to decay as it propagates further upstream. At time=7/8T, the newly formed wave has almost the shape of the original wave and the cycle repeats. The wave is completely attenuated at a distance of 80% of the chord, after which the pressure profile shows no variation over time. Wave peaks are connected by a dashed line showing the upstream propagation of the waves. The suction surface follows a similar process. A wave is formed and propagated upstream with decaying values as it moves further upstream into the channel. The instants at which this wave is formed are however different on the suction surface from those on the pressure surface and there is a phase lag between the two waves. The peak values of the pressure wave on the suction surface are lower than those on the pressure surface and the extent of propagation seems to be limited to a chord-wise distance of 8% from the trailing edge. The slope of the dashed line on Figures 4.6a and 4.6b gives the propagation speed of the pressure wave on the pressure surface.

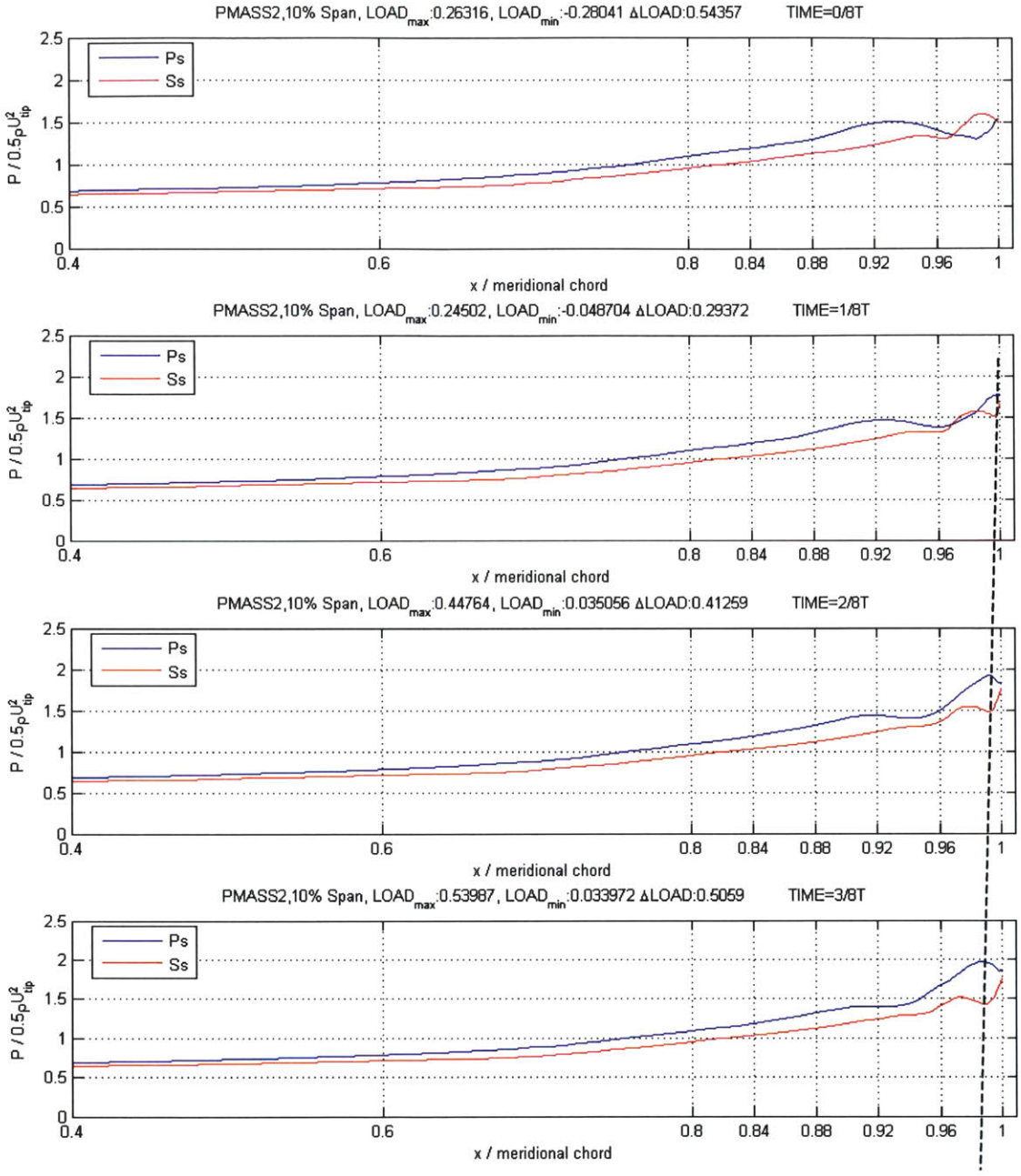

Figure 4.6a: Evolution of pressure waves acting upon main blade surfaces: Pressure (Ps) and Suction (Ss)

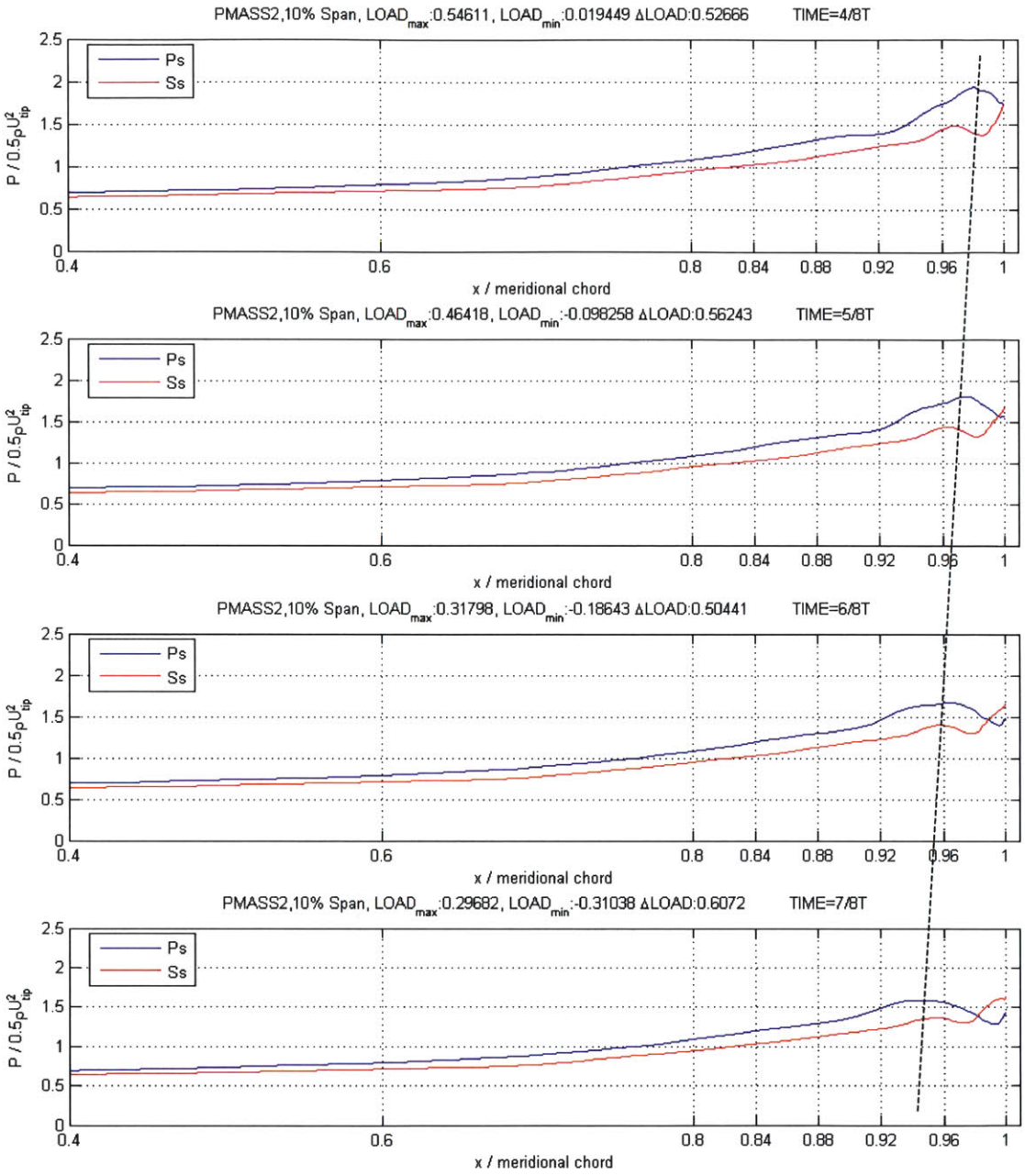

Figure 4.6b: Evolution of pressure waves acting upon main blade surfaces: Pressure (Ps) and Suction (Ss)

The level of loading on the impeller blades is accentuated because pressure waves are propagated differently on the pressure surface and the suction surface of the impeller blade. A remaining issue is the quantification of the speed and wavelength of such waves.

Any disturbance in the pressure field will propagate with the local speed of sound. Since the disturbance propagates in the moving flow exiting the impeller, the speed of the waves with respect to the walls of the blade will be that of sound minus the relative velocity of the flow in the channel. To prove this supposition, the peak of a wave acting on the pressure surface is followed in time over the full period and the value of its mean velocity is computed. Then the velocity of the wave is compared to the value of the local speed of sound minus the relative velocity of the flow (a-W). Both a and W are computed at the exit of the impeller yielding a good estimate although their value is different for different locations inside the channel. The analysis is performed at span locations from hub to mid-span of the blade since at locations near the shroud the presence of a wave is not so evident (see Fig. 4.2). The results are shown in Figure 4.7:

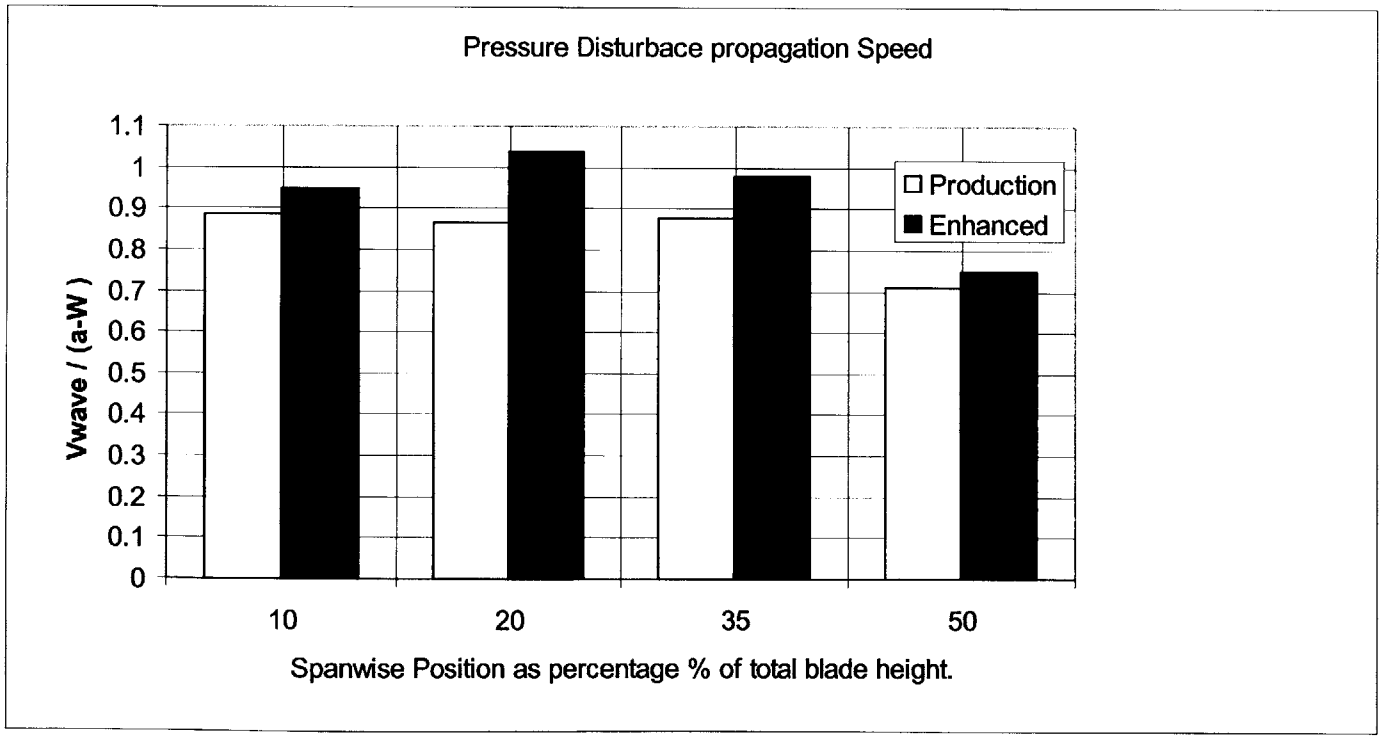

Figure 4.7: comparison of measured wave speed to (a-W) at different spanwise positions

In both compressors, the speed of the wave appears to be very close to a-W. It can be concluded that the propagation of the pressure waves derived from impeller-diffuser interaction depends on the local speed of sound and the relative velocity of the flow within the channel.

An additional metric in the characterization of the pressure wave is the wavelength. (see figure 4.8 below):

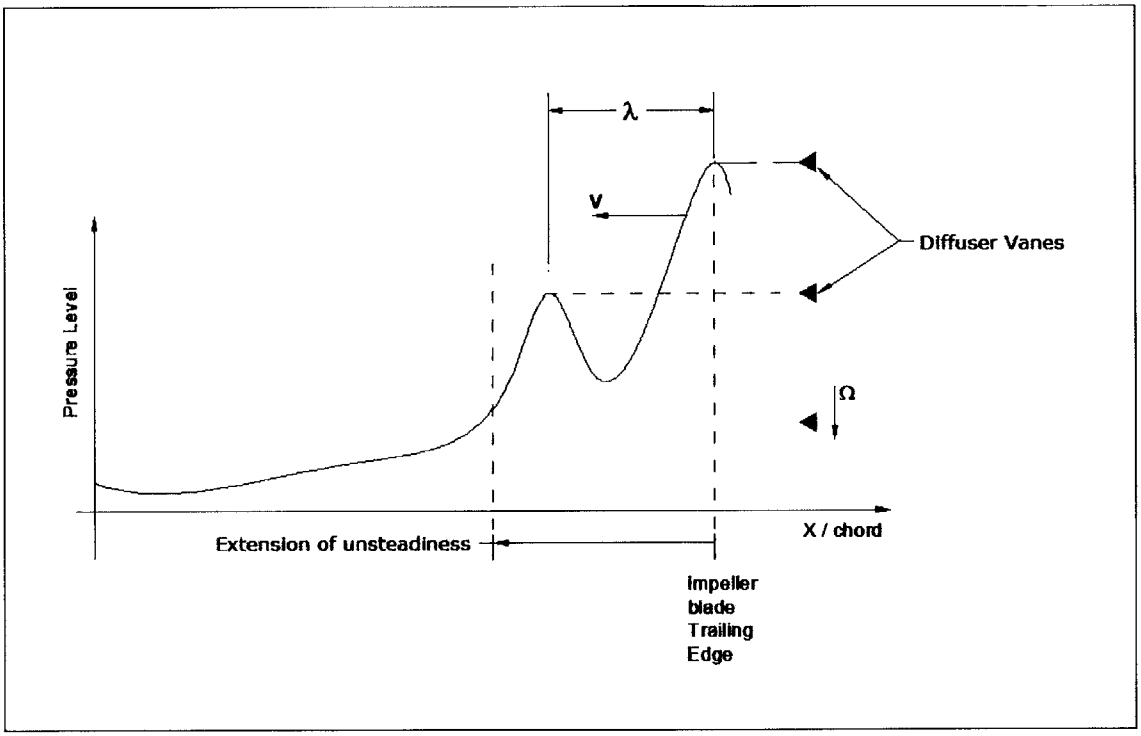

Figure 4.8: Characterization of the pressure waves acting on the surfaces of the impeller blades

A peak in the pressure wave begins when the diffuser vane is aligned with the impeller blade. The wave then travels with a certain speed into the channel as its magnitude is attenuated. The length between two successive peaks should thus be given by the time it takes a new wave to be formed and the speed at which the previous wave has propagated. Thus the wavelength λ is:

$$\lambda = (a - w)T_{Diff} \tag{4.1}$$

Where Tdiff is the time it takes for a diffuser vane to occupy the position of a previous vane when seen from the impeller (i.e. the vane passing period), and $(a\text{-}W)$ is the speed of the wave. In order to prove this supposition, wavelengths are computed. For the baseline case of Production at MASS2, the length between successive peaks was measured and compared to the value predicted by equation 4.1. The measured values are within 10% from the computed values.

The observations made so far are summarized as follows:

- Unsteady loading is formed by the action of pressure waves that propagate along the surfaces of the blades and these originate from the interaction of the impeller with the vanes of the diffuser.

- The extent of propagation is larger on the pressure surface than on the suction surface and is usually confined to a 20% impeller chord from the impeller trailing edge (see section 4.2).

- The waves propagate at a speed approximately given by $a\text{-}W$ and the wavelength is given by $\lambda = (a - w)T_{Diff}$.

4.4 THE DIFFUSER AS THE SOURCE OF UNSTEADINESS

In section 4.3 the unsteady pressure distribution in the pressure surface and the suction surface of the impeller blades were described and quantified. The spatial pressure distribution in the vicinity of the diffuser vane leading edge was identified as the source of the pressure disturbances. It is thus of interest to examine the flowfield at the inlet of the diffuser for the Production and the Enhanced compressor. This will enable to establish a link between the perceived differences in the aeromechanic response and the differences in the unsteady loading between the two compressors.

In her study, Smythe [17] outlined the differences in the time-averaged incidence angle as the possible causes of the aeromechanic response difference between the two compressors. Incidence angle is defined as the difference in the flow angle and the vane angle, both taken with respect to the radial direction. (see Fig 4.9).

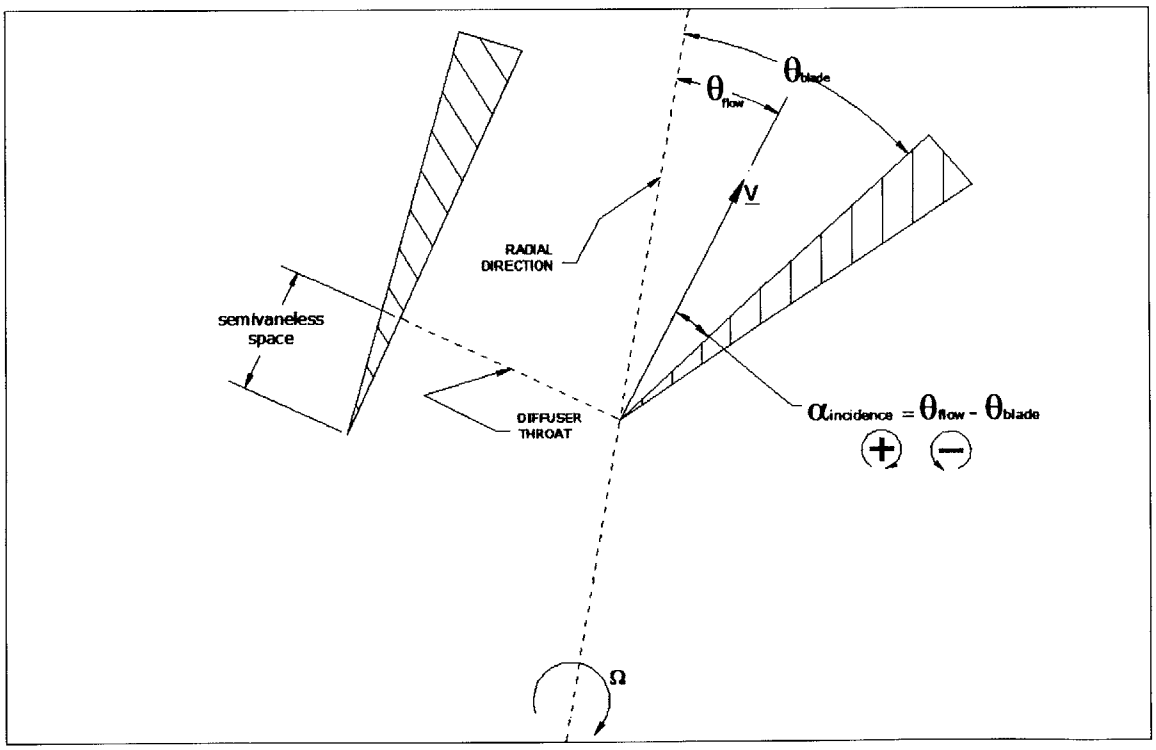

Figure 4.9: Definition of incidence angle and nomenclature of diffuser passage regions

The following figures show velocity triangles for both compressors computed from mass averaged and time averaged quantities at the different points of operation. At every point of operation, both compressors rotate at the same amount of RPM's and the tip speed of the impeller (base of the triangle) is almost identical for the two cases (slightly higher for Enhanced due 0.5% radius enlargement). The Enhanced compressor presents a higher tangential angle θ_t than the Production. The difference resides in a lower value of relative velocity (W_2) for the Enhanced case. A higher value of diffusion is present in the Enhanced compressor (trend given by Figure 4.4 and the de-Haller coefficient. Note de-Haller is always lower for Enhanced than for Production). For the same compressor, since the angle of backsweeping is fixed, it can be concluded that low relative (thus radial) velocities will correspond to higher flow angles. Higher diffusion can be explained by two aspects: higher effective flow area (see section 3.4) and higher density of the flow at the exit of the Enhanced case. In this case, higher effective area (less blockage) has proven to be the dominant effect since the changes in effective area from the Enhanced compressor to the Production are one order of magnitude higher than the difference in density.

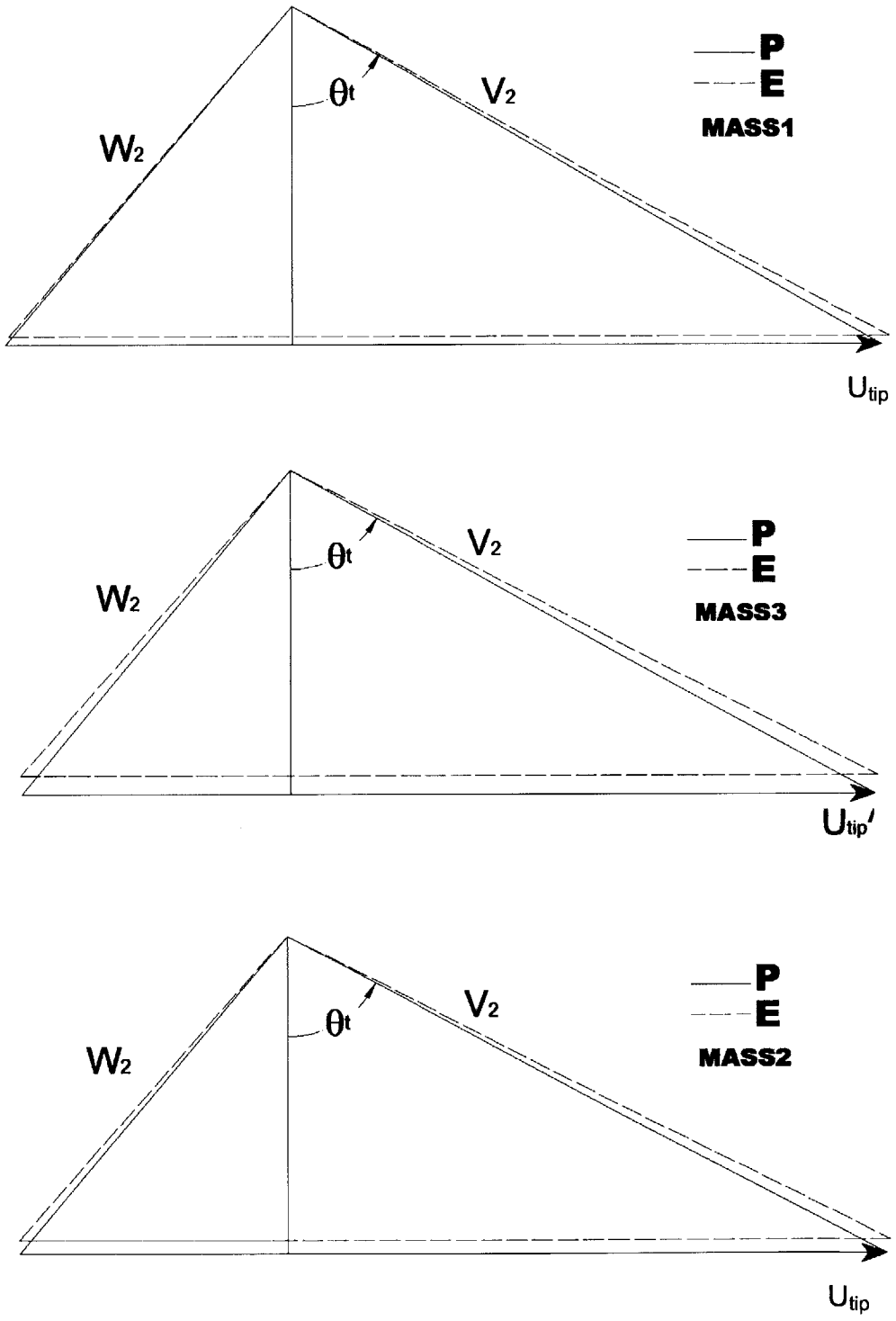

Figure 4.10: Velocity triangles computed at the exit of the impeller with time and mass averaged values of velocity.

When the incidence angle of the flow is high and almost aligned with the diffuser vanes, a streamtube leaving the impeller will see an increase in area as it reaches the semi-vaneless space (see Figure 4.11). The accompanying effect is a rise in static pressure within this region. If the incidence angle is low (sometimes even negative), the streamtube has a reduced area in the semi-vaneless space before entering the diffuser throat. The consequence is a drop in pressure in the semivaneless region.

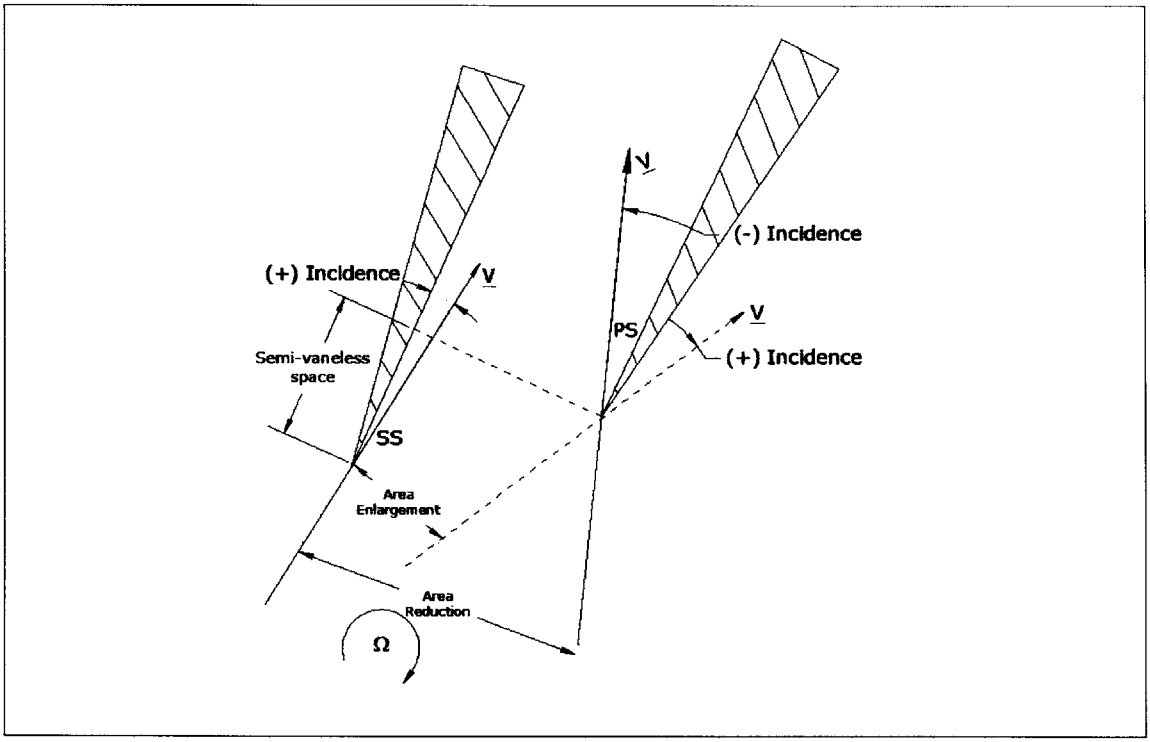

Figure 4.11: Effect of incidence angle in the entering streamtube and the pressure distribution along the semivaneless space.

In figure 4.11 it is demonstrated that less negative incidence at the pressure surface and less positive incidence at the suction surface will produce higher pressure values (larger area). An analysis is conducted by measuring and averaging the values of pressure and incidence angle along the span of the leading edge of the diffuser vane at both pressure and suction surfaces. Values are obtained every 8^{th} of the diffuser vane passing period for a total of 12 points. The results are shown in Figure 4.12.

On the pressure surface, a higher incidence angle (less negative) should be followed by a higher value in pressure from the arguments above. This trend is perceived as the values of the incidence angle change every instant in time. The incidence angle in the Enhanced case is always higher than that of the Production and is thus also accompanied by a higher level in pressure.

At the suction surface the incidence angle is always positive (see Fig 4.12). It can be noticed than in most of the cases the pressure value is low when the incidence angle is high and vice versa. From the trends shown, it is concluded that values of static pressure are changed by the values of the incidence angle.

Table 4.2 is a summary of the observed results for both compressors. The following inferences can be made: The incidence angle in the suction surface of the diffuser vane is similar on each point of operation for the Production and Enhanced compressor with equivalently similar values of static pressure near this zone. On the pressure surface however, incidence angle is considerably different between the Production case and the Enhanced; the incidence angle is less negative for the Enhanced compressor and thus higher values of pressure are registered. This difference is explained from the velocity triangles which show that the flow angle for the Enhanced compressor is always higher. As the point of operation is changed to lower mass flow regimes, the radial value of velocity is increasingly lower. The effect is that the flow angle, hence the incidence angle, is reduced and the pressure on the leading edge of the diffuser vane is increased. MASS2 is expected to show the highest values of pressure and this is the trend that table 4.2 is showing.

		Pressure Surface		Suction Surface		Loading	
		α incidence (range)	P_{max}	α incidence (range)	P_{min}	Δ (P_{max} - P_{min})	$\frac{\Delta enha}{\Delta prod}$
MASS1	Production	-25 to -18	2.72	9 to 7	2.30	0.417	1.8
	Enhanced	-18 to -10	3.03	9 to 7	2.27	0.757	
MASS3	Production	-24 to -16	2.77	12 to 9	2.20	0.568	1.6
	Enhanced	-16 to -7	3.08	12 to 10	2.20	0.882	
MASS2	Production	-23 to -14	2.51	12 to 10	2.15	0.355	3.3
	Enhanced	-18 to -5	3.23	11 to 9	2.08	1.156	

Table 4.2: Summary of span-wise averaged incidence angle and static pressure (normalized) for the three points of operation.

The ratio of pressure difference from pressure surface to suction surface of the two compressors is similar to the ratio of amplitude of loading in the main impeller blade of the two compressors (see tables 4.1 and 4.2) at MASS1 and MASS3. Results of pressure ratio at the diffuser vane leading edge for MASS2 are higher however than those of loading at the same mass flow. Evidence suggests that the levels of pressure at the leading edge of the vane of the diffuser set the levels of loading in the impeller blades and these levels of pressure are highly affected by the value of the incoming flow angle (or incidence angle). This confirms Smythe's[17] supposition on the influence of the incidence angle in the pressure field.

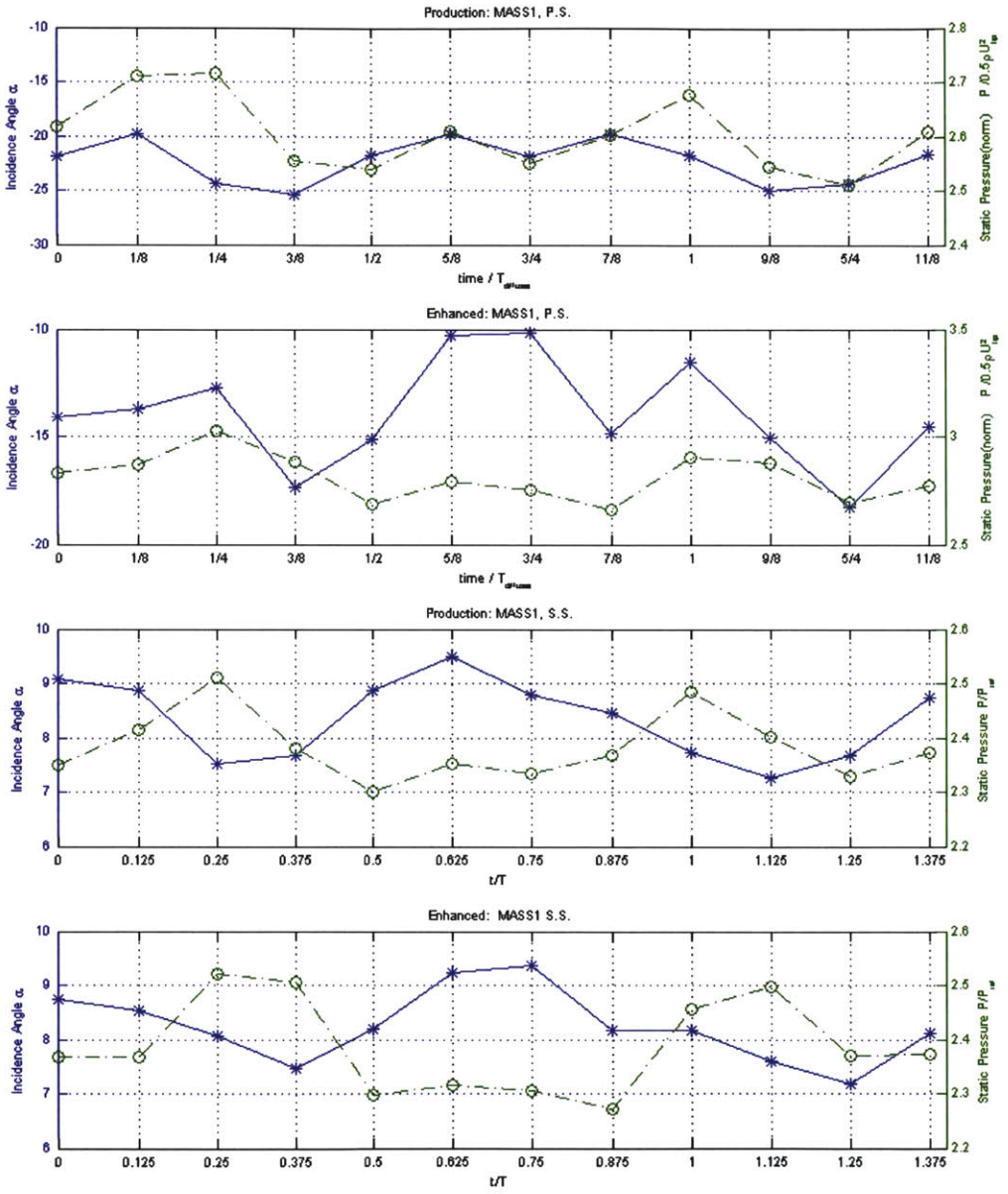

Figure 4.12a: Incidence angle and Pressure level at diffuser vane tip for different time instants (suction and pressure surface): MASS1

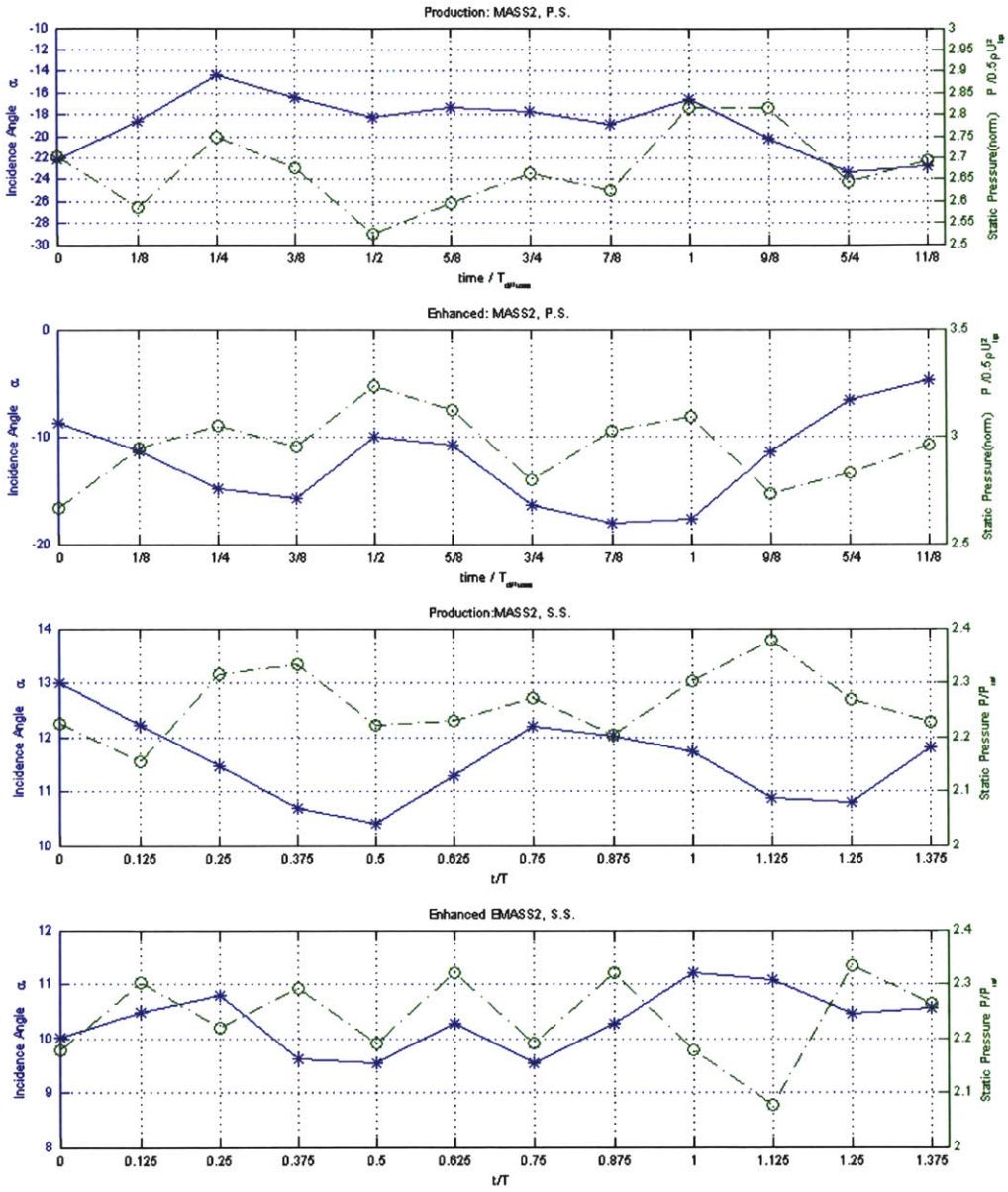

Figure 4.12b: Incidence angle and Pressure level at diffuser vane tip for different time instants (suction and pressure surface): MASS2

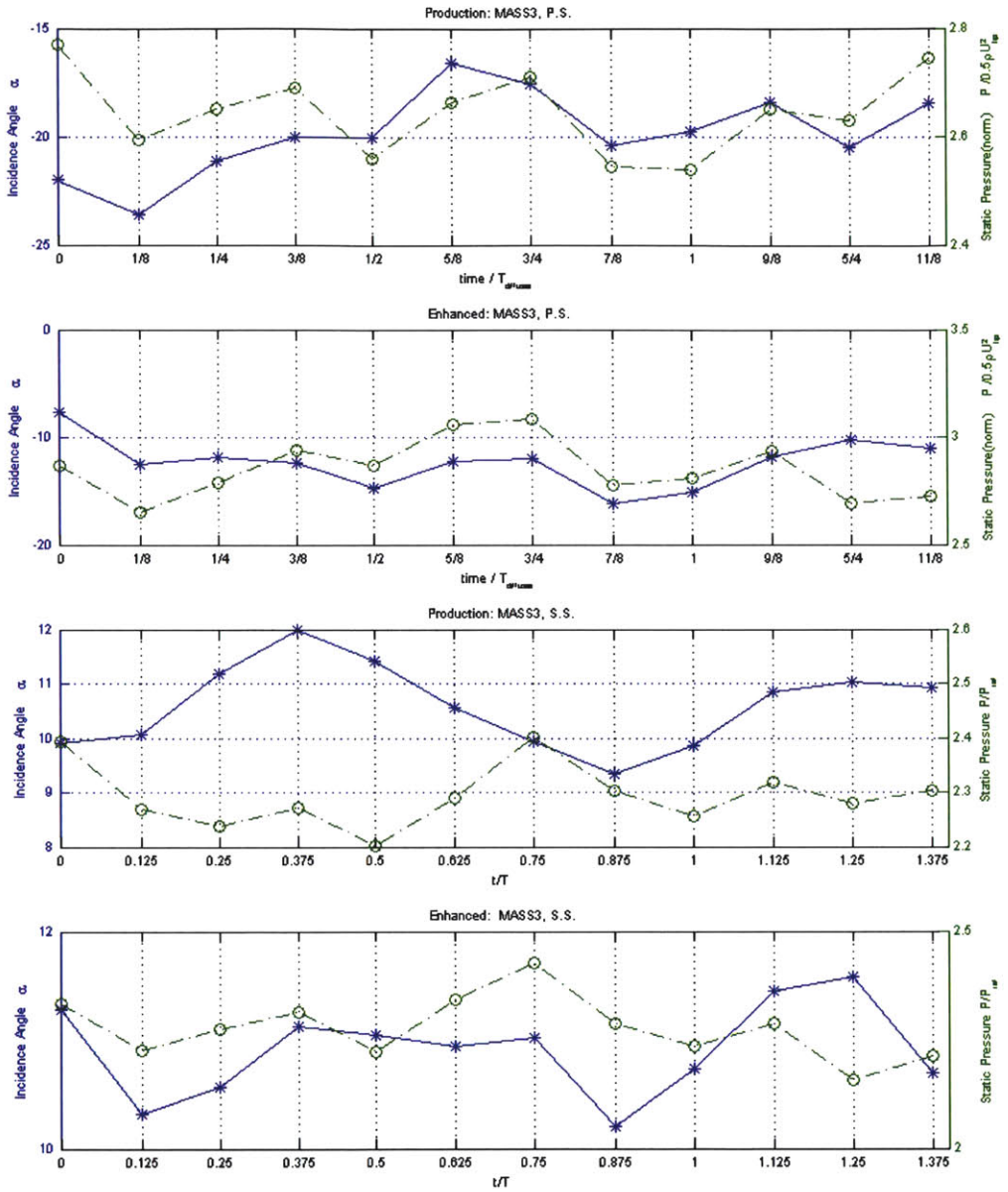

Figure 4.12c: Incidence angle and Pressure level at diffuser vane tip for different time instants (suction and pressure surface): MASS3

4.5 SUMMARY

The study of the unsteady pressure field of the Production and the Enhanced compressor has revealed important features in the understanding of the difference between the two compressors' forcing function. Furthermore, the nature of loading has been characterized. The hypothesis of the influence of the incidence angle on the pressure distribution on the blades of the impeller that was originally posed by Smythe, has been substantiated.

The changes of time-averaged values of pressure in chapter 3 proved to be small in comparison with the unsteady effects. The amplitude of unsteady loading of the Enhanced compressor reached values twice as high as that of the Production (~1.8). This trend suggests that the unsteady effects are important as a forcing function and have a major influence on the difference in aeromechanic response presented by the two compressors.

It was shown that the unsteady loading on the impeller blades originates from pressure waves propagating with a phase difference on the suction and pressure surfaces of the blades. The extent of propagation into the impeller channel appears to increase with the impeller blade loading (Gould [26]). It was also noted that these pressure waves propagate with a speed that is given by the difference in the local values of the speed of sound and the relative velocity. The frequency is set by vane passing frequency and spatial distribution is set by diffuser inlet pressure distribution and vane passing period.

The difference in static pressure existing in the leading edge of the vanes of the diffuser set the level of unsteady loading on the blades of the impeller. This difference in pressure correlate with the incidence angle of the flow into the diffuser which changes with the point of operation and from the Production compressor to the Enhanced compressor. This is in accord with the hypothesis put forward by Smythe [17].

CHAPTER 5

Summary and Conclusions

5.1 SUMMARY

The unsteady 3-D computed flow field for two centrifugal compressors of nearly identical design at three operating points has been post-processed and interrogated to assess: i) the difference in the time averaged performance, ii) the difference in the characteristics of unsteady loading on the blades of the impeller and iii) the flow mechanisms and processes that are responsible for the observations in i) and ii). The three points of operation were chosen as follows: one operating point near design, one at a low corrected mass flow near the compressor stall point and one at a corrected mass flow approximately midway between the first two.

5.2 CONCLUSIONS

The key conclusions of this work are:

- The computed difference in the time-average performance between the Enhanced and Production compressor is due to the change in the level of loss and blockage resulting from the difference in the strength of impeller-diffuser interaction.

- It was shown that the unsteady component of loading on the impeller blade originates from pressure waves propagating with a phase difference on the suction and pressure surfaces of the blades. These waves propagate with a speed that is given by the difference in the local values of the speed of sound and the relative velocity of the flow in the impeller. The frequency of the waves is set by the diffuser vane passing period and the wavelength by the product of the diffuser vane passing period and the speed of the wave. The extent of propagation upstream of the impeller blade trailing edge, appears to increase with impeller blade loading (Gould [26]).

- It was shown that the difference in static pressure from the pressure surface to the suction surface at the leading edge of the diffuser vanes sets the amplitude of unsteady loading on the main blades of the impeller. The level of pressure on both surfaces of the vane is set by the value of the local angle of incidence. The angle of incidence was shown to vary with the point of operation and with compressor design. The difference of incidence angle from the Enhanced compressor to the Production is the result of the changes in the effective impeller channel area produced by a different level of impeller-diffuser interaction. These findings prove the hypothesis originally put forward by Smythe [17].

5.2 RECOMMENDATIONS FOR FUTURE WORK

The following research tasks are recommended for future research efforts:

- Make use of CFD analysis to determine the shape of the unsteady forcing function in the operation of the Enhanced compressor and combine it with FEA to perform a modal force analysis in order to asses the resulting levels of strain. This will provide with a methodology to measure the impact of the changes in design on the aeromechanic response.

- Interrogate what are the causes that produce a reduction in the attenuation extent of unsteadiness associated with the level of diffusion.

REFERENCES

[1] Cumpsty, N.A. *Compressor Aerodynamics*, Krieger, Malabar FL 2004

[2] Greitzer et al, *Internal Flow Concepts and Applications*, Cambridge University Press 2004

[3] Kerrebrock, J. *Aircraft Engines and Gas Turbines*. MIT Press, Cambridge MA, London 2001

[4] Shaw, C.T. *Using Computational Fluid Dynamics*, Prentince Hall, Great Britain 1992

[5] Dean R.C. and Senoo Y., *Rotating Wakes in Vaneless Diffusers*, Trans ASME Journal of Basic Engineering 82: 1960

[6] Eckard D., *Instantaneous Measurements in the jet wake discharge flow of a Centrifugal Compressor Impeller*, Trans ASME Journal of Engineering and Power 97: 1975

[7] Krain H., *A Study on Centrifugal Impeller and Diffuser Flow*, ASME 81-GT-9, May 1981

[8] Ziegler K.U., etal, *A Study On Impeller-Diffuser Interaction: Part I-Influence on the Performance*, ASME GT-2002-30381, June 2002

[9] Chen,J.P, Celestina M.L. and Adamczyk, *A New Procedure for Simulating Unsteady Flows Through Turbomachinery Blade Passages* , ASME 94-GT-151, June 1994

[10] Chen J.P. and Barter, J., *Comparison of Time-Accurate Calculations for the unsteady Interaction in Turbomachinery*, AIAA-98-3292, 1998

[11] Wang,X.,and Chen, J.P., *A post-processor to render Turbomachinery Flows Using Phase-Lag Simulations*. Mississippi State University

[12] Chen J.P., and Briley,W.R., *A new parallel Flow Solver for Unsteady Multiple Blade Row Turbomachinery Simulations*, ASME 2001-GT-0384 June 2001

[13] Dawes W.N., *A Simulation of the Unsteady Interaction of a Centrifugal Impeller With its Vaned Diffuser: Flow Analysis*. ASME Journal of Turbomachinery 117: April 1995

[14] Mansour M., and Kruse M., *Time Unsteady Impeller- Diffuser Interaction on Gas Turbines Engines*, Proceedings of the 5th National Turbine Engine High Cycle Fatigue Conference, Chandler AZ March 7,2000

[15] Rabe D.C., Kenyon J.A. and C. Hah, *Inlet Temperature Distortion Effects on Unsteady Blade Loading in a Transonic Fan*, ISABE 99-7297,1999

[16] Lovely, D. and Haimes, R., *Shock Detection from Computational Fluid Dynamics Results*, AIAA-99-32-85. 1999.

[17] Smythe, C., *Forced Response Predictions in Modern Centrifugal Compressor Design*, Master Thesis, MIT 2005

[18] Shum Y. K. P., *Impeller-Diffuser Interaction in Centrifugal Compressors*, PhD Thesis, MIT 1999

[19] Wallace R., *Modal Response of a Transonic Fan Blade to Periodic Inlet Pressure Distortion*, Master Thesis, Virginia Polytechnic Institute 2003

[20] NASA Technical Memorandum 101067, *PLOT3D User's Manual*, March 1990

[21] Smythe. Honeywell, Internal Report, *Component Design Document*

[22] Khalid, S.,*The Effects of Tip Clearance on Axial Compressor Pressure Rise*,PhD Thesis, MIT 1995

[23] Erdos J.I., Alzner E., and McNally W., *Numerical Solution of Periodic Transonic Flow Through a Fan Stage*, AIAA Journal 15 (11), pp 1559-1568, 1997

[24] Adamczyk, J. J., *Model Equation for Simulating Flows in Multistage Turbomachinery*, ASME 85-GT-226. 1984

[25] Murray, N., *Effects of Impeller-Diffuser Interaction on Centrifugal Compressor Performance*, Master Thesis, MIT 2003.

[26] Gould, K., *Characterization of Unsteady Flow Processes in a Centrifugal Compressor Stage*, Master Thesis, MIT 2006.

[27] Shapiro, A., *The Dynamics and Thermodynamics of Compressible Flow* The Ronald Press Company, New York, USA, 1953